iScience

CellPress
OPEN ACCESS

Article

Selective Survival of Sim1/MC4R Neurons in Diet-Induced Obesity

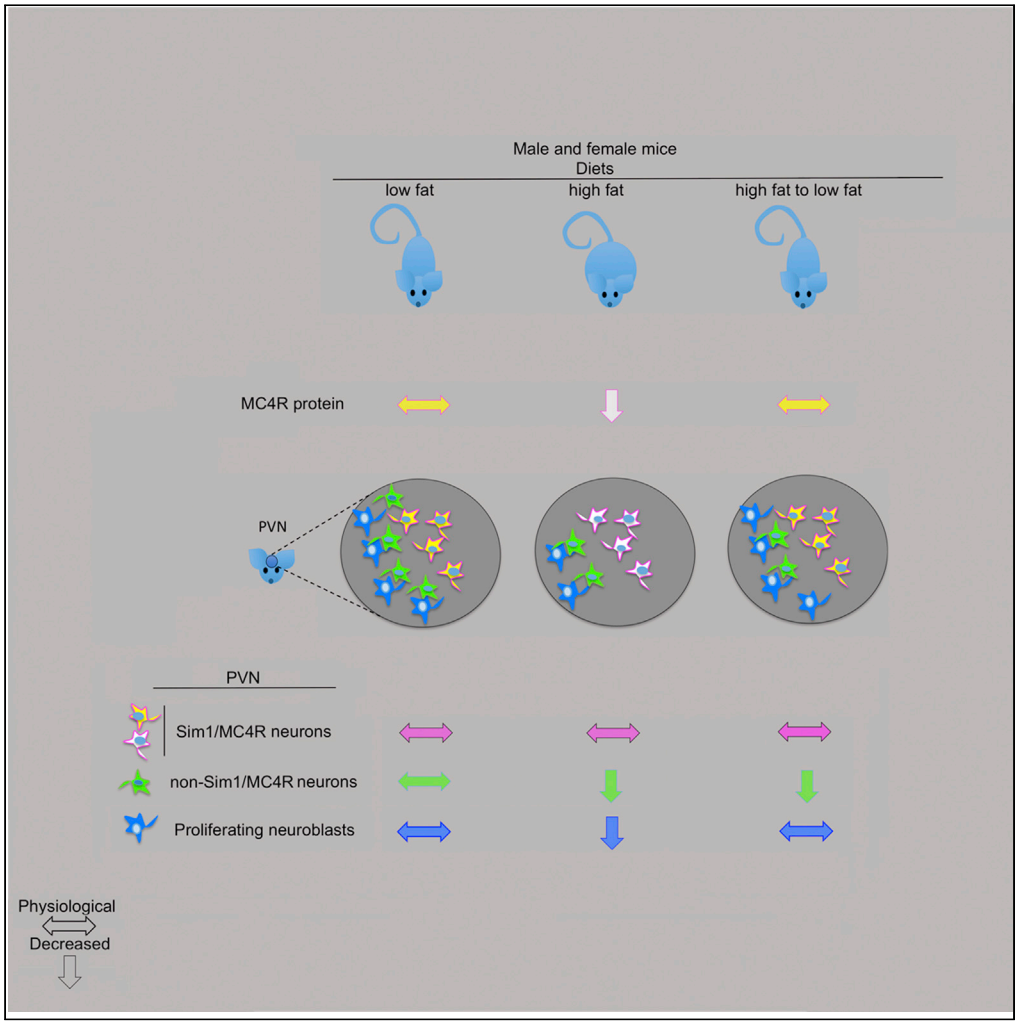

Eugene Nyamugenda, Haven Griffin, Susan Russell, ..., Ishrar Islam, Kevin D. Phelan, Giulia Baldini

gbaldini@uams.edu

HIGHLIGHTS

MC4R localizes to post-synaptic sites along neuronal processes

In PVN of mice with DIO, MC4R neurons survive, but non-MC4R neurons are decreased

In PVN of mice with DIO, MC4R neurons have loss of mitochondria and of MC4R protein

When mice with DIO return to normal weight, abundance of MC4R protein is restored

Nyamugenda et al., iScience *23*, 101114
May 22, 2020
https://doi.org/10.1016/j.isci.2020.101114

iScience

CellPress
OPEN ACCESS

Article

Selective Survival of Sim1/MC4R Neurons in Diet-Induced Obesity

Eugene Nyamugenda,[1] Haven Griffin,[1] Susan Russell,[1] Kimberly A. Cooney,[1] Nicholas S. Kowalczyk,[1] Ishrar Islam,[1] Kevin D. Phelan,[2] and Giulia Baldini[1,3,*]

SUMMARY

In the melanocortin pathway, melanocortin-4 receptor (MC4R) functions to control energy homeostasis. MC4R is expressed in a sub-population of Sim1 neurons (Sim1/MC4R neurons) and functions in hypothalamic paraventricular nuclei (PVN) to control food intake. Mapping sites of hypothalamic injury in obesity is essential to counteract the disease. In the PVN of male and female mice with diet-induced obesity (DIO) there is neuronal loss. However, the existing subpopulation of PVN Sim1/MC4R neurons is unchanged, but has a loss of mitochondria and MC4R protein. In mice of both sexes with DIO, dietary intervention to re-establish normal weight restores abundance of MC4R protein in Sim1/MC4R neurons and neurogenesis in the PVN. However, the number of non-Sim1/MC4R neurons in the PVN continues to remain decreased. Selective survival and recovery of Sim1/MC4R neurons after DIO suggests these neurons as preferential target to restore energy homeostasis and of therapy against obesity.

INTRODUCTION

The melanocortin pathway to control appetite in the hypothalamus includes POMC neurons in the arcuate nucleus and single-minded family basic-helix-loop-helix transcription factor 1 (Sim1) neurons localized to the paraventricular nuclei (PVN) (Baldini and Phelan, 2019). The population of Sim1 neurons in the PVN includes neurons that co-express melanocortin-4 receptor (MC4R) (Sim1/MC4R neurons) and other neurons that lack MC4R and express prodynorphin (Andermann and Lowell, 2017; Balthasar et al., 2005; Li et al., 2019; Shah et al., 2014). POMC neurons project from the arcuate nucleus to PVN of the hypothalamus to release α-MSH, which binds to melanocortin-4 receptor (MC4R), a G-protein-coupled receptor (GPCR) expressed by Sim1/MC4R neurons to decrease food intake (Andermann and Lowell, 2017; Baldini and Phelan, 2019; Balthasar et al., 2005; Li et al., 2019; Toda et al., 2017). In mice, increased dietary fat content induces hypothalamic injury, increases caloric intake, and promotes onset of obesity. Identifying sites of hypothalamic injury in mice with diet-induced obesity (DIO) and discovering underlying mechanisms of injury is considered essential to counteract onset of obesity and its recurrence in humans.

Male rodents treated with high-fat (HF) diet (HFD) have inflammation, gliosis, and neuronal loss, as well as altered response to leptin and insulin in the mediobasal hypothalamus (De Souza et al., 2005; Dorfman and Thaler, 2015; Thaler et al., 2012; Timper and Bruning, 2017; Velloso et al., 2009). Accumulation of saturated fat in the hypothalamus induces inflammatory signaling in the microglia, which contributes to mitochondrial dysfunction in POMC neurons (Kim et al., 2019; Paeger et al., 2017; Valdearcos et al., 2014, 2017; Yi et al., 2017). In POMC neurons of male rodents, exposure to HFD decreases contact sites between mitochondria and the ability of the endoplasmic reticulum (ER) to process POMC to generate and secrete α-MSH, and synapse formation (Cakir et al., 2013; Enriori et al., 2007; Horvath et al., 2010; Schneeberger et al., 2013, 2015; Thaler et al., 2012). Female mice have injury to the mediobasal hypothalamus to a lesser degree, by mechanisms that include decreased microglial activation and estrogen-dependent protection of POMC neurons (Dorfman et al., 2017; Qiu et al., 2018). Thus, in the mediobasal hypothalamus, glial activation and inflammation are major inducers of damage to hypothalamic POMC neurons.

In the arcuate nucleus, profound injury by exposure to HFD takes place in male but not in female mice. Differently, we have found that DIO induces in PVN injury to Sim1 neurons and neuronal loss in both male and female mice to a similar extent (Nyamugenda et al., 2019). Local microgliosis, although evident in the arcuate nucleus, does not take place in the PVN (Nyamugenda et al., 2019). In DIO, steroidogenic

[1]Department of Biochemistry and Molecular Biology, University of Arkansas for Medical Sciences, Little Rock, AR 72205, USA

[2]Department of Neurobiology & Developmental Sciences, University of Arkansas for Medical Sciences, Little Rock, AR 72205, USA

[3]Lead Contact

*Correspondence: gbaldini@uams.edu

https://doi.org/10.1016/j.isci.2020.101114

factor (SF-1)-expressing neurons localized to the ventromedial hypothalamus become hypersensitive to insulin and contribute to loss of POMC neuron activity (Klockener et al., 2011; Timper and Bruning, 2017). In DIO, MC4R signaling within the melanocortin pathway also becomes over-responsive to MC4R agonists (Enriori et al., 2007). We have proposed that the hyper-responsiveness to MC4R agonist in mice with DIO, rather than being due to increased MC4R expression, is instead another consequence of hypothalamic injury with impaired clathrin-dependent endocytosis and blunted MC4R desensitization (Cooney et al., 2017). Whether and to what extent DIO induces injury to Sim1/MC4R neurons of the PVN and changes expression of MC4R protein is a central question that has not yet been addressed. This work finds that abundance of MC4R protein is reduced by DIO. Moreover, dietary intervention to reverse obesity results in restored MC4R protein abundance likely because of selective survival of the Sim1/MC4R neurons in male and female mice with DIO. Differently, non-Sim1/MC4R neurons are decreased by DIO and restored neurogenesis by dietary intervention is insufficient to replace lost PVN neurons even when mice return to their normal weight.

RESULTS

In the PVN of Male and Female Sapphire Mice with Diet-Induced Obesity, There Is Neuronal Loss, but the Number of Sim1/MC4R Neurons Is Instead Unchanged

Exposure to HFD induces loss of neurons in the arcuate nucleus and decreases α-MSH protein abundance in POMC neurons in male mice (Nyamugenda et al., 2019; Schneeberger et al., 2013; Thaler et al., 2012). Differently, exposure to HFD induces injury to Sim1 neurons and loss of neurons in the PVN of both male and female mice (Nyamugenda et al., 2019). Sim1 neurons in the PVN include the subpopulation of MC4R neurons (Sim1/MC4R neurons), which regulate satiety and body weight (Balthasar et al., 2005; Li et al., 2019). Here, we asked whether exposure to HFD decreases the population of Sim1/MC4R neurons by using Sapphire mice, which express GFP under melanocortin-4 receptor promoter. A group of 8-week-old male Sapphire mice (starting weight = 24.5 ± 0.56 g) and another group (starting weight = 25.4 ± 1.8 g) were treated in parallel with low fat (LF) (control group) and palm oil-based HFD with 45% kcal derived from fat (Nyamugenda et al., 2019), respectively, for a total of 8 weeks. After 7 weeks, all mice were treated with 5-bromo-2′-deoxyuridine (BrdU, 50 mg/kg body weight per day) for 1 week (Figure S1A). Exposure to HFD for 8 weeks increased caloric intake in male (by 28.1 ± 3.9%, $p < 0.0001$) and female mice (by 41.0 ± 10.6%, $p < 0.0001$) (Figures S1B and S1F). After 8 weeks of treatment, exposure to HFD also increased body weight in male and female Sapphire mice (by 30.9 ± 5.4%, $p < 0.0001$ and by 27.8 ± 5.6%, $p < 0.05$, respectively) (Figures S1C and S1G). Male, but not female, Sapphire mice had also increased serum leptin (by 3.7 ± 1.6-fold, $p < 0.001$) (Figures S1D and S1H). Thus, exposure to HFD induces weight gain both in male and female mice, with metabolic effects being more pronounced in male mice. Male, but not female, Sapphire mice exposed to HFD for 8 weeks had reduced α-MSH in the arcuate nucleus (by 70.7 ± 15.4%, $p < 0.001$) (Figures 1A and 1E). Therefore, 8-week exposure of Sapphire mice to HFD induces injury to POMC neurons in the arcuate nucleus of males but not of females. Exposure to HFD decreased the number of NeuN-positive cells in the PVN of male and female mice by 44.2 ± 13.7%, $p < 0.01$ and by 70.6 ± 18%, $p < 0.0001$, respectively (Figures 1B and 1F), indicating neuronal loss at this location. To determine whether in male and female Sapphire mice neuronal loss included the population of Sim1/MC4R neurons, we visualized these neurons by the GFP expressed under the MC4R promoter (Liu et al., 2003). In these mice, GFP is undetectable by direct fluorescence microscopy and is visualized by staining with anti-GFP antibodies. By counting the number of GFP-positive cells, exposure to HFD did not decrease Sim1/MC4R neurons in male and female mice (Figures 1B and 1F).

There is evidence that neurogenesis takes place both in juvenile and adult hypothalamus and that this process is decreased in mice exposed to HFD (Kokoeva et al., 2005; Li et al., 2012; McNay et al., 2012). It is possible that persistence of the entire Sim1/MC4R neuronal population in mice with DIO is because regeneration of these neurons increases under HF feeding conditions and replenishes the lost neurons. In the adult rodent hypothalamus, tancytes localized to the ependymal layer of the third ventricle are neural progenitors (Yoo and Blackshaw, 2018). In neurogenesis, ependymal tancytes undergo proliferation, which can be monitored by BrdU incorporation in DNA, and then migrate as neuronal precursors to the brain parenchyma (Batailler et al., 2014; Matsuzaki et al., 2015; Xu et al., 2005). To monitor this process in Sapphire mice, males and females were given BrdU daily for 7 days by intra-peritoneal injection prior to sacrifice (Figure S1A). In brain sections, BrdU immunostaining revealed robust cell labeling in the ependymal layer, indicating that preferential proliferation of brain tancytes is clearly detectable under our experimental conditions (white arrowheads). BrdU labeling appeared also in the PVN, suggesting the existence of cells that

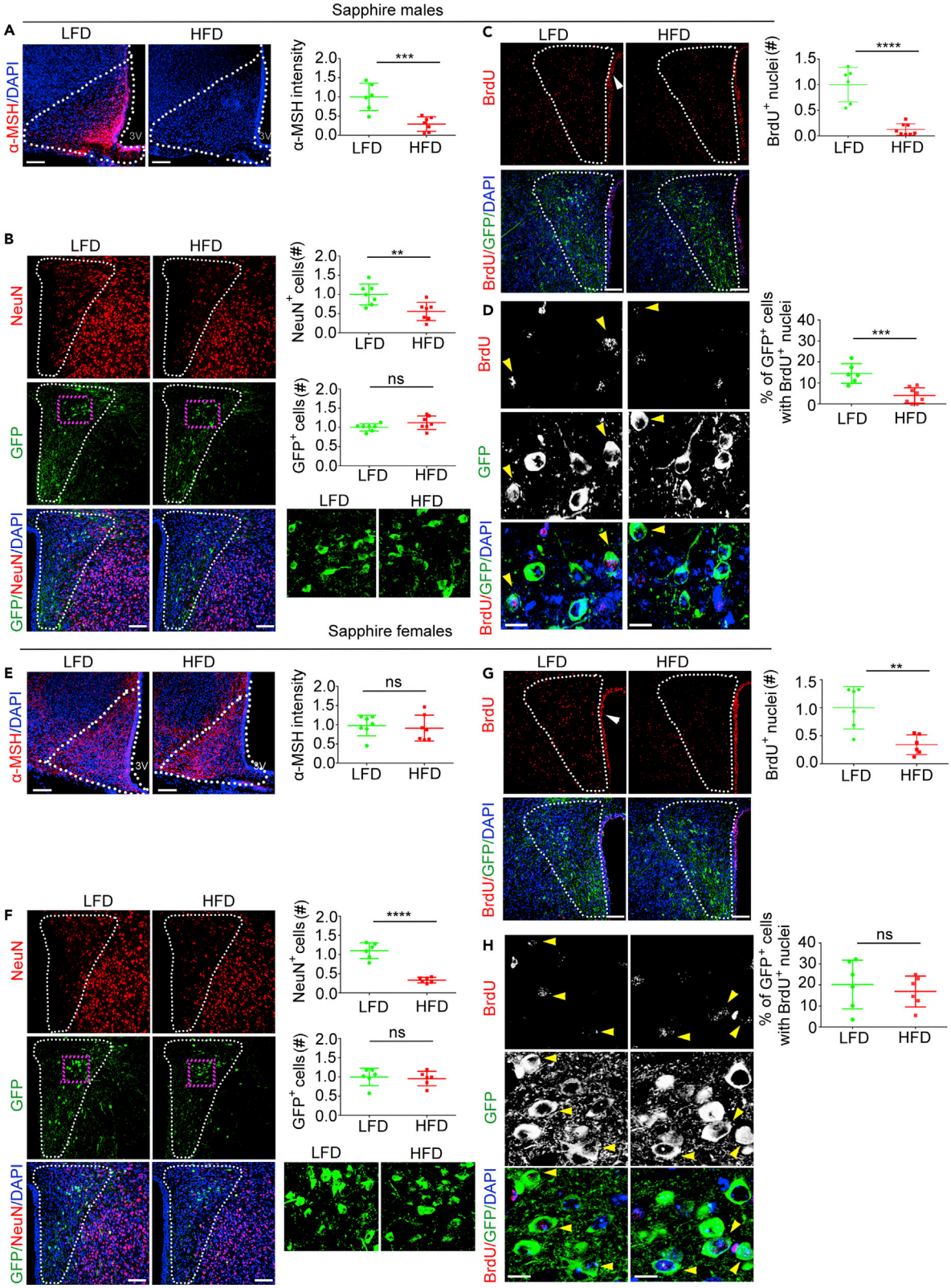
Sapphire males
A
LFD
HFD
α-MSH/DAPI
3V
α-MSH intensity
***
B
NeuN
GFP
GFP/NeuN/DAPI
NeuN+ cells(#)
**
GFP+ cells (#)
ns
C
BrdU
BrdU/GFP/DAPI
BrdU+ nuclei (#)
****
D
% of GFP+ cells with BrdU+ nuclei
***
Sapphire females
E
ns
F
****
ns
G
**
H
ns

Figure 1. In the PVN of Male and Female Sapphire Mice with Diet-Induced Obesity (DIO), There Is Neuronal Loss, but the Number of Sim1/MC4R Neurons Is Instead Unchanged

(A–H) Confocal microscopy of brain sections from male and female Sapphire mice exposed to LF diet (LFD) and HFD (HFD). Males, LFD, n = 6–7 and HFD, n = 6–7; females, LFD, n = 6–7 and HFD, n = 6–7. (A) and (E) Intensity of α-MSH immunostaining in arcuate nucleus derived from four maximum intensity projection (MIP) images per mouse. (B) and (F) Number of NeuN-expressing cells and number of GFP-expressing Sim1/MC4R neurons in the PVN derived from two MIP images per mouse. (C) and (G) Number of BrdU-positive nuclei in PVN derived from two MIP images per mouse. (D) and (H) Percentage of PVN Sim1/MC4R neurons with BrdU-positive nuclei from two MIP images per mouse. Dotted line in (A) and (E) outlines arcuate nucleus; dotted line in (B), (C), (F) and (G) outlines PVN; scale bars in (A–C) and (E–G), 60 μm; scale bars in (D) and (H), 10 μm; data in all graphs are normalized. **p < 0.01, ***p < 0.001; ****, p < 0.0001. Data are represented as mean values +/- SD.

underwent proliferation during the Brdu pulse in the brain parenchyma. By measuring with ImageJ the fluorescence intensity of the BrdU-positive particles, the abundance of BrdU immunostaining per particle was decreased by 30.3% in cells localized to PVN as compared with that of cells localized in the ependymal layer. Thus, in the 3–8 days of chase after the BrdU pulse and before sacrifice (Figure S1A), a fraction of cells localized to PVN may have undergone one more cell division than cells localized to the ependymal layer. In both male and female Sapphire mice with DIO, incorporation of BrdU in the PVN was decreased by 87.3 ± 33.6%, $p < 0.001$ and by 65.9 ± 37.8%, $p < 0.01$, respectively. Thus, DIO induces a decrease of cells localized to PVN that proliferated during or after the 1-week interval of BrdU delivery (Figures 1C and 1G). Next, we asked whether cells that proliferated during the BrdU pulse were also able to differentiate to MC4R neurons. Sapphire mice express GFP under the MC4R promoter, thus allowing identification of these neurons (Liu et al., 2003; Panaro et al., 2014). In male and female mice, nuclear incorporation of BrdU took place in 14.5 ± 4.05% and 20.24 ± 11.57% of the GFP-positive cells, respectively. Thus, PVN Sim1/MC4R neurons regenerate rapidly in male and female Sapphire mice (Figures 1D and 1H). DIO decreased neurogenesis of the Sim1/MC4R neurons by 72.3 ± 25.7%, $p < 0.001$ in male, but not in female, mice (Figures 1D and 1H). Thus, in male mice with DIO, regeneration of Sim1/MC4R neurons is profoundly decreased, whereas the number of Sim1/MC4R neurons is nevertheless maintained. Thus, at least in male mice with DIO, neurogenesis does not appear relevant to maintain the size of Sim1/MC4R neuronal population.

In Sim1/MC4R Neurons of Male and Female Mice, DIO Induces Loss of CoxIV Abundance, Decreased Mitochondria Content, and Extension of Mitochondrial Network

In DIO, Sim1/MC4R neurons, rather than undergoing cell death, may be at earlier stages of neuronal dysfunction. A feature of neuronal degeneration is injury to mitochondria with malfunctions in mitochondrial respiration (Breuer et al., 2013). Cytochrome *c* oxidase (Cox) is a multi-subunit enzyme located in the inner mitochondrial membrane that functions as the terminal component of the electron transport chain. Low levels of subunit IV of Cox (CoxIV) in human peripheral tissues is associated with mitochondrial dysfunction, obesity, and type 2 diabetes (Van der Schueren et al., 2015). To determine whether DIO induces loss of CoxIV in Sim1/MC4R neurons, we measured its cell abundance in matching sections of the hypothalamus derived from Sapphire mice. In male and female mice exposed to HFD, cell abundance of subunit IV of Cox (CoxIV) in Sim1/MC4R neurons of the PVN was decreased (by 60.3 ± 20 .9%, $p < 0.05$ and by 57.3 ± 15.5%, $p < 0.01$, respectively) (Figures 2A and 2C). Mitochondria form networks in different cell types including neurons (Bach et al., 2003), and DIO has been found to disrupt mitochondrial networks in POMC neurons of the arcuate nucleus (Schneeberger et al., 2013). We used superresolution microscopy of CoxIV immunostaining to determine the size of mitochondrial network under normal conditions and DIO in Sim1/MC4R neurons. We reasoned that interconnected mitochondria would appear as a single particle of larger size than a single mitochondrion. We then measured, in GFP-positive cells, the area of CoxIV immunostaining detected as a single particle by the ImageJ analysis tool. To this end, for each condition, mitochondrial particles were divided by size into ten groups (group 1 has particles of smallest size; group 10 has particles of largest size), with each group containing the same number of particles (from LF diet [LFD] mice, 5,923 total particles derived from 104 Sim1/MC4R neurons, 592 particles per group; HFD, 4,556 total particles derived from 118 Sim1/MC4R neurons, 455 particles per group). The same type of analysis was carried out on samples female mice on HFD (LFD, 10,670 particles derived from 103 Sim1/MC4R neurons, 1,067 particles per group; HFD diet, 7,740 particles derived from 103 Sim1/MC4R neurons, 774 particles per group). DIO reduced the size of mitochondrial area within group 10 by 62.2 ± 9.6%, $p < 0.001$ in male mice and by 57.0 ± 13.9%, $p < 0.01$ in female mice (Figures 2B and 2D), thereby suggesting that DIO decreases the extension of mitochondrial network in Sim1/MC4R neurons. HFD also reduced mitochondrial cell coverage area in the Sim1/MC4R neurons of male and female mice by 47. 7 ± 16.2%, $p < 0.05$ and by 46.6 ± 15.4%, $p < 0.05$, respectively (Figures 2B and 2D). Thus, in male and female mice with DIO, there

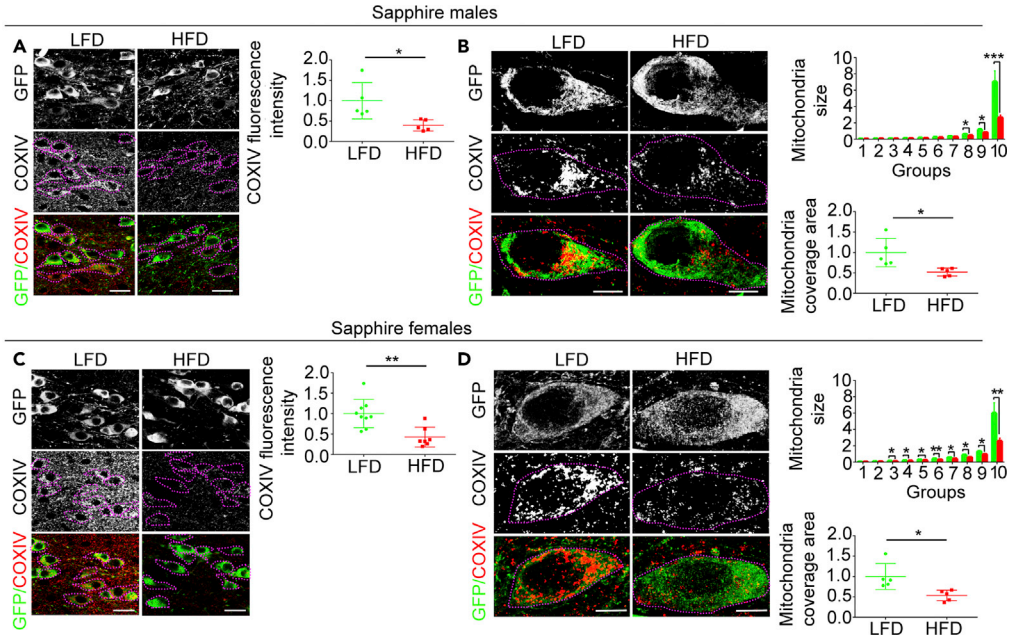

Figure 2. In Sim1/MC4R Neurons of Male and Female Mice, DIO Induces Loss of CoxIV Abundance, Decreased Mitochondria Content, and Extension of Mitochondrial Network

(A–D) Fluorescence microscopy of brain sections from Sapphire mice exposed to LF diet (LFD) and HF diet (HFD). (A) and (C) Intensity of CoxIV immunostaining (red fluorescence) in Sim1/MC4R neurons identified by GFP immunostaining (green fluorescence) in PVN of males (LFD, n = 5 and HFD, n = 5) and females (LFD, n = 8, HFD, n = 7). Each data point was obtained by taking the average of CoxIV intensity from 25 to 30 Sim1/MC4R neurons using five confocal images taken with 60× objective per mouse. Data are normalized; scale bar, 20 μm. (B) and (D) Super-resolution fluorescence microscopy images of sections from male Sapphire mice (LFD, n = 5 and HFD, n = 5) and female Sapphire mice (LFD n = 5 and HFD n = 5). Mitochondria size is in μm^2; mitochondrial coverage area is normalized; scale bar, 5 μm. *$p < 0.05$, **$p < 0.01$, ***$p < 0.001$. Data are represented as mean values +/- SD.

is mitochondrial injury with loss of cell CoxIV, loss of mitochondria, and reduced size of mitochondrial network in Sim1/MC4R neurons.

Exposure to Elevated Palmitate Is Sufficient to Induce Loss of CoxIV and to Disrupt Mitochondrial Function in Primary Hypothalamic Neurons

In DIO, levels of hypothalamic palmitate are increased with activation of microglia, inflammation, and neuronal injury that includes changes in mitochondrial dynamics and disrupted mitochondrial morphology in POMC neurons (De Souza et al., 2005; Thaler et al., 2012; Valdearcos et al., 2014, 2017). However, microgliosis does not take place in the PVN of mice with DIO (Nyamugenda et al., 2019), whereas Sim1/MC4R neurons still develop mitochondrial injury at this location. Exposure of neuronal Neuro2A cells to elevated palmitate has direct effects to promote ER stress and to decrease expression of exogenous MC4R in neuronal cells (Cooney et al., 2017; Cragle and Baldini, 2014; Mohammad et al., 2007). To determine whether exposure to elevated saturated fat induces direct injury to mitochondria, Neuro2A cells expressing HA-MC4R-GFP (Mohammad et al., 2007) were exposed to 250 μM palmitate. In these cells, abundance of ER proteins, detected by KDEL immunostaining, was increased by 68.6%, $p < 0.0001$, whereas abundance of HA-MC4R-GFP and of CoxIV were instead decreased by 46.4%, $p < 0.0001$ and by 25.8%, $p < 0.0001$, respectively (Figures 3A–3D). These data suggest that, in neuronal cells exposed to elevated palmitate, loss of MC4R is paralleled both by ER stress and by loss of CoxIV. Next, we determined whether loss of CoxIV takes place in primary cultures of hypothalamic neurons exposed to elevated saturated fat and associates with mitochondrial dysfunction. To this end, the hypothalamic neurons were incubated without or with 250 μM palmitate for 48 h. Fluorescence intensity of MitoTracker Red CMXRos (MitoTracker) monitors mitochondria membrane potential (MMP) in live cells (Smith et al., 2011). Exposure to elevated palmitate decreased MitoTracker fluorescence intensity per cell by 41.8 ± 22.8%, $p < 0.0001$ (Figures 3E and 3F), indicating loss of capacity to generate MMP. After cell fixation, co-immunostaining of primary hypothalamic

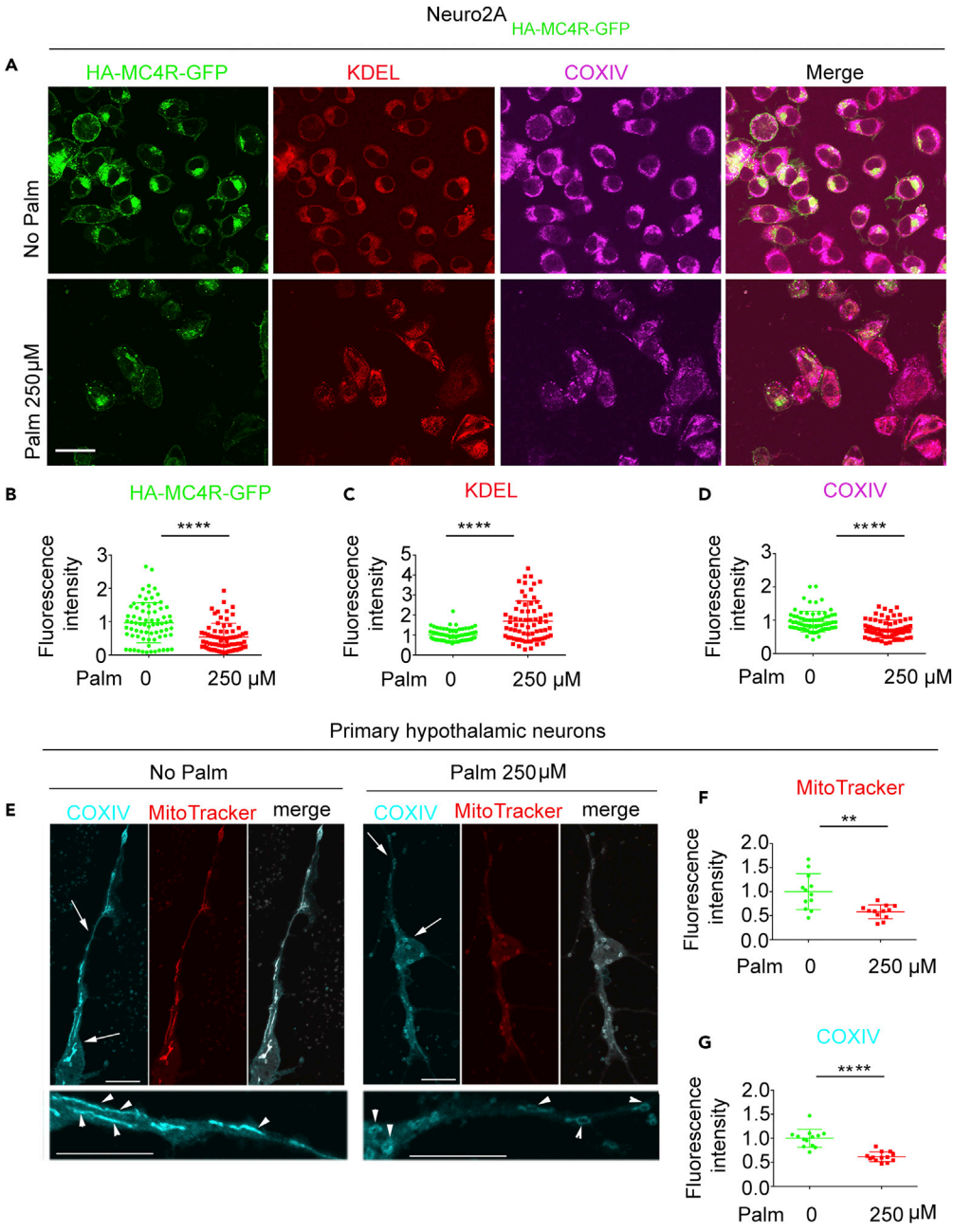

Figure 3. Exposure to Elevated Palmitate Is Sufficient to Induce Loss of CoxIV and to Disrupt Mitochondrial Function in Primary Hypothalamic Neurons

(A–D) Confocal microscopy of Neuro2A cells stably expressing HA-MC4R-GFP and incubated with and without palmitate for 16 h. HA-MC4R-GFP (green), KDEL immunostaining (red), and COXIV immunostaining (magenta). (B–D) Quantification of HA-MCR-GFP fluorescence, KDEL and COXIV immunostaining. Each symbol in graph corresponds to the value measured from one cell (n = 75 cells).

(E–G) Confocal microscopy of primary hypothalamic neurons treated without palmitate or with 250 µM palmitate for 48 h and exposed to MitoTracker for 30 min, fixed and immunostained for CoxIV. (F) Quantification of MitoTracker fluorescence intensity by live microscopy. (G) Quantification of CoxIV immunostaining in images of fixed cells including that in (F). Data from 12 to 13 cells per condition are normalized; scale bars, 10 µm. **$p < 0.01$. **** $p < 0.0001$. Data are represented as mean values +/- SD.

neurons with anti-CoxIV finds that cell abundance of the protein is decreased by 38.4 ± 10.1%, $p < 0.0001$ as compared with that of neurons that were not exposed to the elevated fatty acid (Figures 3E and 3G). These data suggest that exposure of hypothalamic neurons to elevated palmitate has direct effects to reduce CoxIV abundance and to disrupt mitochondrial function.

The *in vitro* data of Figure 3 suggest that DIO may induce in the PVN, in addition to mitochondrial loss, also loss of MC4R protein. Currently, there is a lack of reliable antibodies to detect MC4R protein. Recently, MC4R has been visualized in knockin mice by the addition of a GFP tag placed at the C terminus of the receptor (Siljee et al., 2018). However, immunostaining with antibodies against the GFP tag at the C terminus of the protein did not allow for a direct visualization of MC4R distribution at low magnification to study distribution and abundance of the protein in the brain. We reasoned that a smaller HA tag placed at the C terminus of the receptor together with the use of an enzyme-linked immunoassay for signal amplification might instead monitor MC4R expression in Sim1/MC4R neurons of the PVN and of other brain regions. We have previously shown that HA-MC4R-GFP expressed in Neuro2A cells localizes to the plasma membrane and is continuously internalized by clathrin-dependent endocytosis (Cooney et al., 2017; Mohammad et al., 2007). By using an anti-HA monoclonal antibody, we find that human MC4R with two HA tags placed at the C terminus of the receptor MC4R-HA was also predominantly localized at the intracellular compartment, where it co-localized with clathrin (Figure S2A). When treated with the synthetic MC4R agonist MTII, Neuro2A cells expressing HA-MC4R-GFP and MC4R-HA had increased intracellular cAMP level (by 89.1%, $p< 0.001$% and by 68.9%, $p < 0.01$) (Figure S2B). Dose-response experiments indicated that response to MTII of human MC4R-HA (EC_{50} = 39.81 nM) was similar to that of human MC4R (Srinivasan et al., 2007) and (Figure S2C). Thus, the HA tag does not impair cAMP receptor signaling. CRISPR-Cas9 was used to generate knockin MC4R-HA mice with two HA tags placed at the C terminus of endogenous MC4R (Figure S2D). PCR and DNA sequencing showed that HA peptides were inserted at the C terminus of the endogenous MC4R (Figure S2E). MC4R-HA was detected in PVN sections derived from MC4R-HA$^{+/-}$ mice, but not from wild-type (WT) mice. MC4R-HA also was detectable in other regions of the brain known to express MC4R mRNA such as the lateral olfactory tract (LOT); CA1, CA2, CA3 of the hippocampus; medial preoptic area (MPO); medial amygdala (MeA); dorsal motor nucleus of vagus (DMV); and supraoptic nucleus (SON) (Figures 4A and S2F) (Liu et al., 2003). Next, we tested the cellular localization of MC4R-HA. MC4R-HA immunostaining was at the cell body and at processes of PVN neurons. At locations outside and inside of the PVN (red and cyan boxes, respectively, Figure 4B) MC4R-HA was found at discrete sites, with some appearing along neuronal processes (cyan arrowheads). Some of the MC4R-HA sites co-localized with PSD95 (magenta and white arrowheads at low and high magnification, respectively), thereby suggesting that a fraction of cell receptor localizes to post-synaptic sites. To validate at the single cell level expression of MC4R-HA in Sim1/MC4R neurons, MC4R-HA mice were crossed with Sapphire mice to obtain Sapphire:MC4R-HA mice (Figure 4C). MC4R-HA was expressed at the cell body of PVN neurons that also expressed GFP (magenta arrows) and at some (orange arrowheads) but not all (magenta arrowheads) neuronal processes (Figure 4C). Axons from Sim1/MC4R neurons project out of the PVN to reach the parabrachial nucleus (Li et al., 2019). To further explore whether MC4R-HA localizes to neuronal processes of Sim1/MC4R neurons, we crossed Sim1-Cre$^{+/-}$: Rosa-mEGFP$^{+/+}$ with MC4R-HA$^{+/+}$ mice to obtain Sim1-Cre$^{+/-}$: Rosa-mEGFP$^{+/-}$: MC4R-HA$^{+/+}$ mice. In these mice, membrane-bound EGFP (mEGFP) appeared as bright green fluorescence at the cell membrane of Sim1/MC4R neurons and along processes projecting outside of the PVN. MC4R-HA was expressed at the cell body (Figure 4D, white arrowheads) and at discrete sites of long processes that appear to represent axons of Sim1/MC4R neurons coursing through neighboring regions outside of the PVN (cyan arrows, Figure 4D, and at higher magnification, magenta arrowheads Figure 4E). To determine whether axons of Sim1/MC4R neurons have post-synaptic sites, we prepared primary hypothalamic neurons from the Sim1-Cre $^{+/-}$: Rosa-mEGFP$^{+/-}$ mice (n neurons = 10). The Sim1 neurons in primary culture extend short processes morphologically identified as dendrites (orange arrows) and one long process (~0.4 mm), identified as an axon, where PSD95 was accumulated at discrete spots (Figure 4F). Together, data suggest that Sim1/MC4R neurons have post-synaptic sites along axons.

DIO Induces Loss of MC4R-HA Specific to PVN in Male and Female MC4R-HA$^{+/-}$ Mice

It is possible that, although signaling of tagged MC4R-HA appears unchanged as compared with that of MC4R (Figure S2), yet the HA tag might disrupt some other receptor properties relevant to appetite control. To test that, we compared food intake by adult male and female MC4R-HA$^{+/-}$ and WT mice

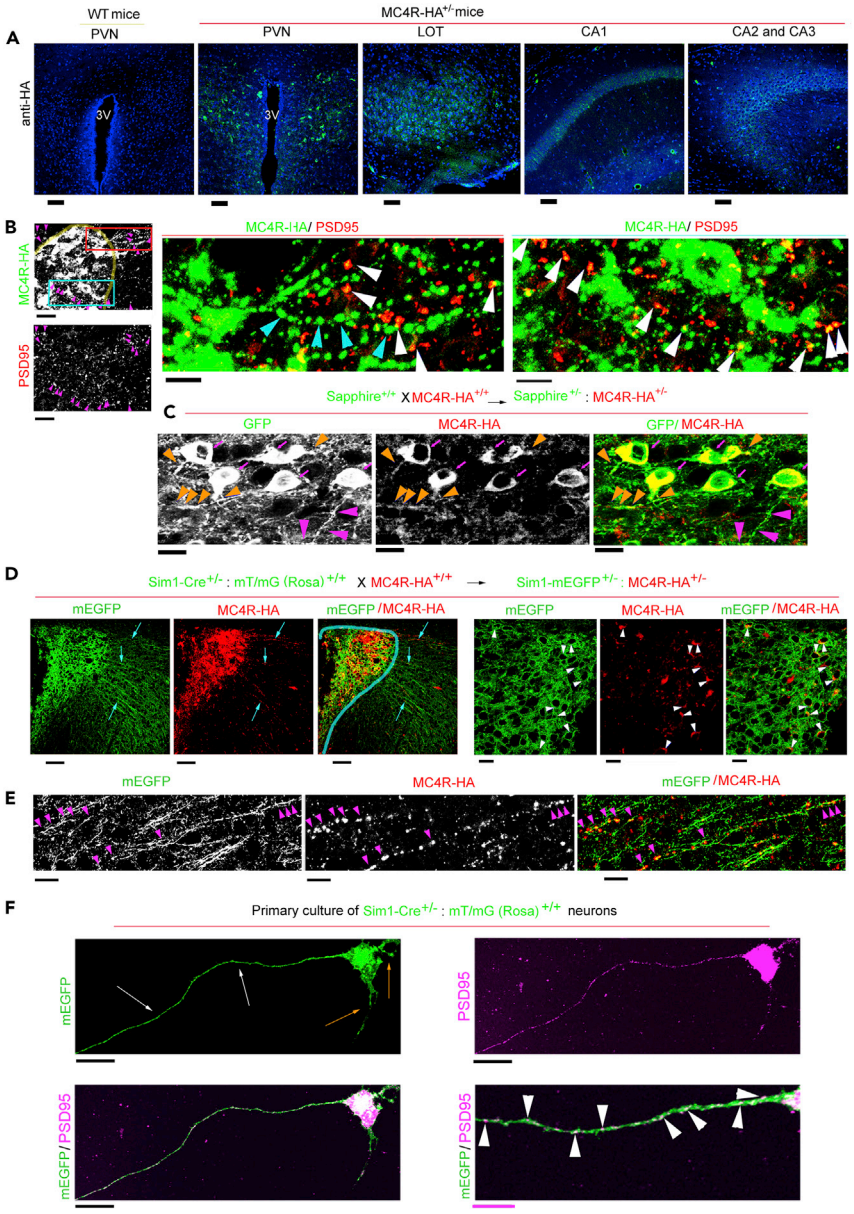

Figure 4. In MC4R-HA$^{+/-}$ Mice, MC4R-HA Protein Is Expressed in Sim1/MC4R Neurons, Where it Localizes to Post-Synaptic Sites of Neuronal Processes

(A) Confocal microscopy of brain sections derived from wild-type (WT) and MC4R-HA$^{+/-}$ mice immunostained with anti-HA. 3V, third ventricle; LOT, lateral olfactory tract; CA1, CA2, CA3, hippocampus regions 1, 2, and 3; scale bar, 60 μm.

(B) HA (green fluorescence) and PSD95 (red fluorescence) immunostaining of brain sections that include the PVN (outlined by a yellow line) derived from MC4R-HA$^{+/-}$ mice; a region outside PVN (red box) and a region inside PVN (cyan box) shows sites of MC4R-HA and PSD95 at low magnification; scale bar, 40 μm. The region outside of PVN (red line) and inside PVN (cyan line) are shown at higher magnifications in the two right panels; scale bar, 20 μm; sites of MC4R-HA immunostaining with (white arrowheads) and without (cyan arrowheads) co-localization with PSD95.

(C) Confocal microscopy of brain sections from Sapphire$^{+/-}$:MC4R-HA$^{+/-}$ mice. Magenta arrows, HA immunostaining in the soma of Sim1/MC4R neurons expressing GFP; orange arrowheads, HA immunostaining in processes of Sim1/MC4R neurons expressing GFP; magenta arrowheads, processes of Sim1/MC4R neurons lacking HA immunostaining. Scale bar, 10 μm.

(D) Confocal microscopy of brain sections from Sim1-Cre$^{+/-}$: Rosa-mEGFP$^{+/-}$:MC4R-HA$^{+/-}$ mice. In Sim1/MC4R neurons expressing mEGFP (green), HA immunostaining (red) is detectable at neuronal processes (indicated by cyan arrows) projecting outside the PVN (indicated by cyan line); scale bar, 80 μm. At increased magnification, HA immunostaining localizes to cell bodies of Sim1/MC4R neurons expressing mEGFP; scale bar, 10 μm.

Figure 4. *Continued*

(E) At high magnification, MC4R-HA localizes to neuronal processes of Sim1/MC4R neurons projecting from the PVN (scale bar, 10 μm).

(F) PSD95 immunostaining in primary hypothalamic Sim1 neurons derived from Sim1-Cre$^{+/-}$: Rosa-mEGFP$^{+/-}$ mice. Orange arrows indicate processes morphologically identified as dendrites, and white arrows indicate a process morphologically identified as axon. Black scale bars, 20 μm. At higher magnification, white arrowheads indicate sites of PSD95 accumulation along the axon. Magenta scale bar, 5 μm.

(Figure S3A). At 8 weeks of age, when weight and food intake started being recorded, knockin heterozygous male and female MC4R-HA$^{+/-}$ mice were heavier than their WT siblings by 13.2 ± 4.0%, $p < 0.0001$ and by 11.0 ± 6.2%, $p < 0.01$, respectively (Figures S3C and S3J). Thus, tagged MC4R-HA induces mild increase in body weight at young age. However, for the following 8 weeks, food intake and percentage weight gain of male and female MC4R-HA$^{+/-}$ mice were not different from those of WT mice (Figures S3D, S3E, SK, and SL). We then asked whether exposing male and female MC4R-HA$^{+/-}$ mice to HFD for 8 weeks starting at 8 weeks of age increased caloric intake and weight gain (Figure S3B). In male and female MC4R-HA$^{+/-}$ mice, exposure to HFD increased caloric intake by 40.0 ± 8.8%, $p < 0.0001$ and 38.6 ± 6.2%, $p < 0.0001$, respectively (Figures S3F and S3M), body weight by 55.8 ± 13.6%, $p < 0.0001$ and 45.6 ± 3.4% $p < 0.0001$, respectively (Figures S3G and S3N), and blood glucose by 11.3 ± 5.3%, $p < 0.05$, and 36.4 ± 7.6%, $p < 0.001$, respectively (Figures S3H and S3O). Exposure to HFD induced in male, but not in female mice, increased insulinemia by 3.7 ± 1.1-fold, $p < 0.0001$ (Figures S3I and S3P). Thus, HF feeding induces in MC4R-HA$^{+/-}$ mice increased caloric intake likely contributing to increased weight and altered metabolism. Next, we asked whether DIO decreases MC4R in Sim1/MC4R neurons by using MC4R-HA$^{+/-}$ mice exposed to LFD and HFD as in Figure S3. The brain was harvested at sacrifice and matched brain sections were immunostained with the anti-HA antibody. Regions of interest (ROIs) of the same areas were drawn to outline the PVN. Exposure to HFD decreased MC4R-HA fluorescence pixel density in the PVN of male and female MC4R-HA$^{+/-}$ mice by 66.3 ± 25.1%, $p < 0.0001$ and by 76.5 ± 19.0%, $p < 0.0001$, respectively (Figures 5A and 5D). Conversely, in the same brain sections, MC4R-HA fluorescence intensity in LOT and SON were unchanged (Figures 5B, 5C, 5E, and 5F). Together, these data indicate that, in male and female mice, DIO induces loss of MC4R protein abundance specific to the PVN.

In Male and Female MC4R-HA$^{+/-}$ Mice with DIO, Switching to an LFD Decreases Caloric Intake, Restores Normal Weight, and Reverts Hepatosteatosis

When WT mice with DIO are returned to LFD, they lose weight and have restored leptin sensitivity in the arcuate nucleus of the hypothalamus (Cakir et al., 2013; Enriori et al., 2007; Timper et al., 2018). To determine whether MC4R-HA$^{+/-}$ mice with DIO also return to normal weight upon dietary intervention, two cohorts of 8-week-old animals were exposed for 8 weeks to LFD and to HFD, respectively. Mice exposed to LFD at the beginning of the diet treatment remained on the LFD for the entire duration of the study. Differently, at 16 weeks of age, one group of mice derived from the cohort of MC4R-HA$^{+/-}$ mice fed with the HFD continued to remain on the HFD, whereas another group was switched to the LFD. Mice remained on these diets for another 4 weeks until the end of the study (Figure 6A). In the week immediately following the switch of diet from HF to LF male and female mice with DIO dropped their caloric intake (by 51.5 ± 18.8%, $p < 0.01$ and 42.9 ± 9.9%, $p < 0.05$ respectively) and then, after another week, returned to the same caloric intake as that of mice constantly kept on the LFD (Figures 6B and 6H). After switching the diet from HF to LF, male and female mice with DIO returned to the same weight as that of mice constantly fed with LFD within 1 and 2 weeks, respectively (Figures 6C and 6I). Four weeks after switching male and female mice with DIO from HF to LFD, leptin concentration in serum collected at sacrifice was at the same level as that of mice kept constantly on the LFD and decreased by 2.6 ± 0.47-fold, $p < 0.0001$ and by 2.4 ± 0.7-fold, $p < 0.001$, respectively, as compared with that of mice constantly kept on HFD (Figures 6D and 6J). Four weeks after switching the diet from HF to LF, male serum insulin was at the same level as that of male mice kept constantly on the LFD and decreased by 1.9 ± 0.5-fold, $p < 0.05$ as compared with that of male mice constantly kept on HFD (Figure 6E). Differently, in female mice with DIO exposed to the switch of diet from HF to LF, insulin serum level was increased by 2.1 ± 0.4-fold, $p < 0.01$, as compared with that of female mice that received LFD for the entire duration of the study (Figure 6K). Exposure to HFD induces altered lipid metabolism, which results in hepatosteatosis in humans and rodents (Nam et al., 2017; Rosqvist et al., 2014). In livers of male and female MC4R-HA$^{+/-}$ mice kept on HFD liver abundance of lipid droplets visualized by Nile Red staining was increased by 4.8 ± 1.4-fold, $p < 0.0001$ and by 4.7 ± 1.7-fold, $p < 0.001$, respectively, as compared with that of mice constantly kept on LFD (Figures 6F and 6L). We have found that, in mice exposed to HFD, loss of the ER chaperone Grp78/BiP in pericentral hepatocytes parallels hepatosteatosis (Trentzsch et al., 2020). Abundance of Grp78/BiP in pericentral hepatocytes of male and female MC4R-HA$^{+/-}$ mice was decreased by 89.0 ± 48.4%,

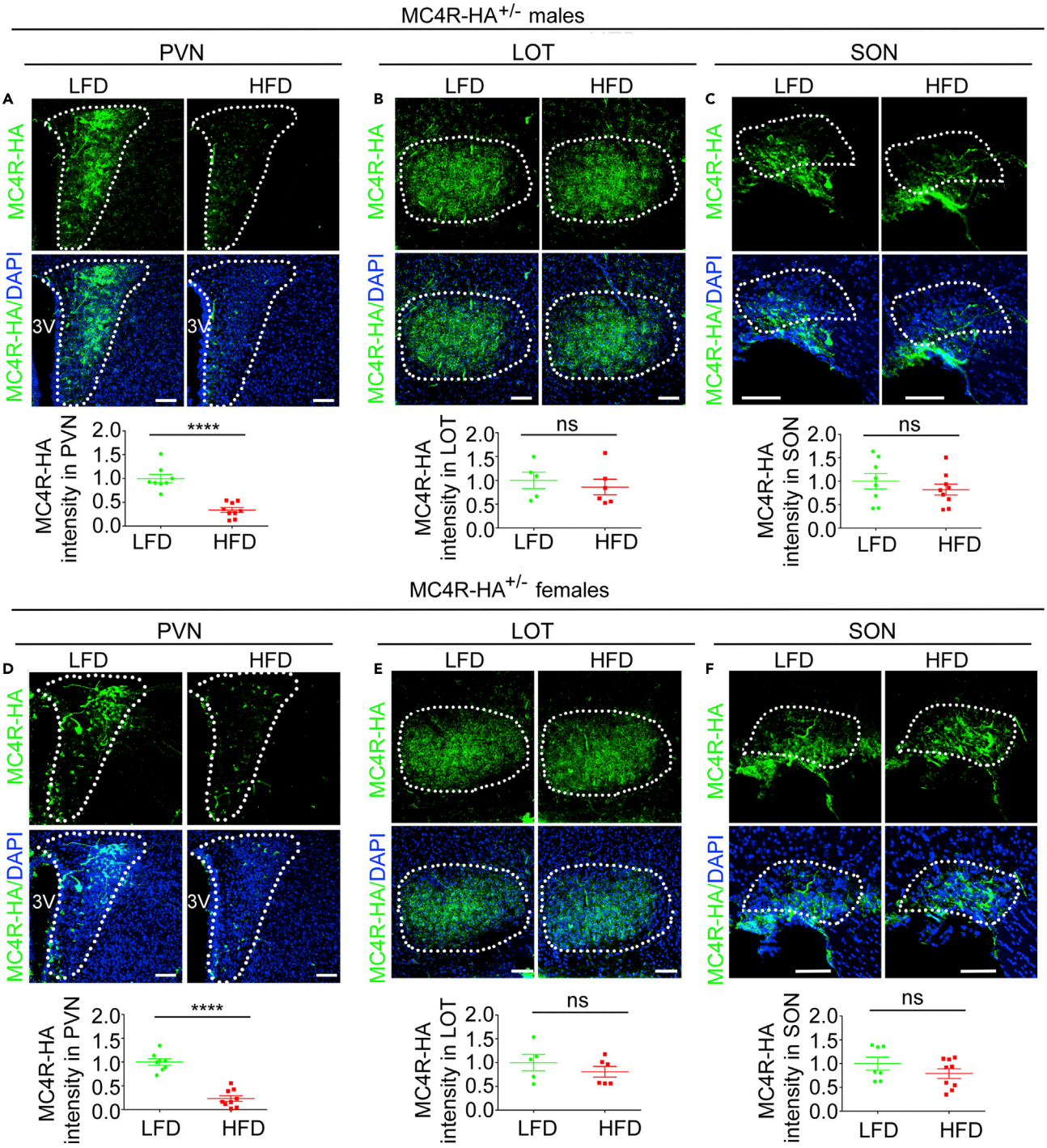

Figure 5. DIO Induces Loss of MC4R-HA Specific to PVN in Male and Female MC4R-HA$^{+/-}$ Mice

(A–C) Confocal microscopy of brain sections derived from male MC4R-HA$^{+/-}$ mice immunostained with anti-HA. PVN, LFD, n = 8 and HFD, n = 9 (A); LOT, LFD, n = 5, HFD, n = 6 (B); SON, LFD, n = 8, HFD, n = 9 (C).

(D–F) Confocal microscopy of brain sections derived from female MC4R-HA$^{+/-}$ mice immunostained with anti-HA. PVN, LFD, n = 8, HFD, n = 9 (D); LOT, LFD, n = 5, HFD, n = 6 (E); SON, LFD, n = 7, HFD, n = 9 (F). Data were from 4 MIP per mouse; data in graphs are normalized; scale bar, 80 μm. ****, p<0.0001. Data are represented as mean values +/- SD.

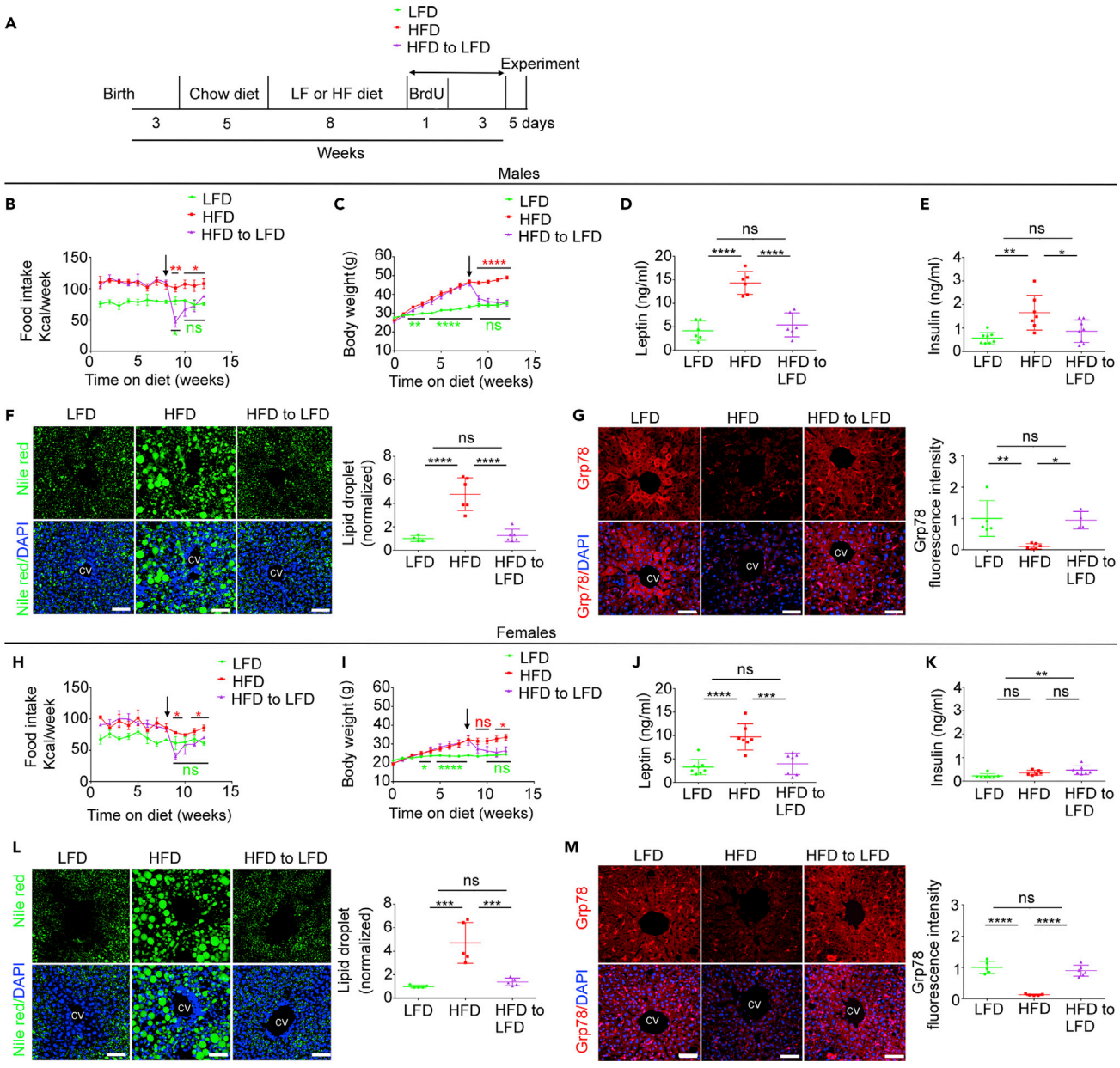

Figure 6. In Male and Female MC4R-HA$^{+/-}$ Mice with DIO, Switching to a LF Diet Decreases Caloric Intake, Restores Normal Weight, and Reverts Hepatosteatosis

(A) Timeline.

(B–G) Male MC4R-HA$^{+/-}$ mice, arrow shows time of diet switch; food intake and body weight, LFD, n = 8, HFD, n = 10, HFD to LFD, n = 10 (B–E); serum leptin, LFD, n = 6, HFD, n = 6, HFD to LFD, n = 6 (D); serum insulin, LFD, n = 8; HFD, n = 7; HFD to LFD, n = 8 (E); (F–G) Confocal microscopy of liver, normalized data are from three MIP images per mouse; liver lipid droplets, LFD, n = 4, HFD n = 6, HFD to LFD, n = 6 (F); liver Grp78, LFD, n = 5; HFD, n = 6, HFD to LFD diet n = 4 (G). (B and C) Data are represented as mean values +/- SEM. (D–G) Data are represented as mean values +/- SEM.

(H–M) Female MC4R-HA$^{+/-}$ mice, arrow shows time of diet switch; food intake and body weight, LFD, n = 9, HFD, n = 7, HFD to LFD, n = 8 (H–I); serum leptin, LFD, n = 8; HFD, n = 7; HFD to LFD, n = 7 (J); serum insulin, LFD, n = 7; HFD, n = 6; HFD to LFD, n = 7 (K). (L and M) Confocal microscopy of liver, normalized data are from three MIP images per mouse; liver lipid droplets, LFD, n = 5, HFD n = 5, HFD to LFD, n = 5 (L); liver Grp78, LFD, n = 5; HFD, n = 6, HFD to LFD, n = 6 (M). Scale bars, 60 μm. *p < 0.05, **p < 0.01, ***p < 0.001; ****, p < 0.0001. (H and I) Data are represented as mean values +/- SEM. (J–M) Data are represented as mean values +/- SEM.

$p < 0.01$ and by 87.0 ± 20.0%, $p < 0.0001$, respectively, as compared with that of mice constantly kept on LFD (Figures 6G and 6M). Four weeks after switching the diet from HF to LF, the liver lipid droplet content and expression of GrP78/BiP in pericentral hepatocytes of male and female mice returned to the same level as that of mice kept on the LFD for the entire duration of the study (Figures 6F, 6G, 6L, and 6M). Thus, MC4R-HA$^{+/-}$ male and female mice with DIO, when switched to LFD, reduce their caloric intake, lose weight, and have normal levels of hepatic lipid and ER chaperone content, as well as normalized leptin levels. However, female mice that returned to normal weight after DIO have hyper-insulinemia, whereas male mice under the same conditions have normalized insulin levels. Overall, data indicate similarity of MC4R-HA$^{+/-}$ mice and WT mice exposed to HF feeding to revert adverse metabolic effects by DIO upon dietary intervention.

In the PVN of Male and Female MC4R-HA$^{+/-}$ Mice with DIO, Change of Diet Restores Neurogenesis

It is possible that, when mice return to their normal weight after DIO, neurogenesis replaces lost PVN neurons. To monitor neurogenesis upon dietary change, male and female MC4R-HA$^{+/-}$ mice were given daily 50 mg/kg BrdU during the first week immediately after the switch of diet from HF to LF (Figure 6A). In male and female MC4R-HA $^{+/-}$ mice exposed to HFD, nuclear BrdU staining was decreased in the PVN by 62.41 ± 27.83%, $p < 0.05$ and by 41.91 ± 31.69%, $p < 0.05$, respectively, as compared with mice kept on LFD. Thus, exposure to HFD decreases cell proliferation (Figures 7A and 7C). When the diet of male and female MC4R-HA $^{+/-}$ mice was switched from HF to LF, PVN BrdU staining increased to the same level as that of mice constantly kept on the LFD (Figures 7A and 7C). Thus, switching diet from HF to LF resumes cell proliferation in the PVN of male and female mice. Doublecortin (DCX) is a microtubule-associated protein transiently expressed in migrating neuroblasts and a suitable marker of neurogenesis in adult mice (Ayanlaja et al., 2017; Brown et al., 2003). To determine whether, in male and female MC4R-HA$^{+/-}$ mice treated with HFD, there is reduced neurogenesis of PVN neurons, we co-stained sections with antibodies against DCX and BrdU. In matching brain sections of male and female MC4R-HA $^{+/-}$ mice treated with HFD, the number of DCX- and BrdU-positive cells in PVN was decreased by 75.79 ± 19.93%, $p < 0.01$ and by 69.46 ± 27.03%, $p < 0.01$, respectively, as compared with those of mice kept on the LFD (Figures 7B and 7D, magenta arrowheads). Thus, HF feeding induces loss of neurogenesis in PVN. Conversely, when male and female MC4R-HA $^{+/-}$ mice with DIO were given LFD, DCX- and BrdU-positive cells in PVN were increased to the same levels as those of mice constantly kept on the LFD (Figures 7B and 7D). These experiments indicate that replacing HFD with LFD restores proliferation of neuroblasts and their migration to the PVN.

In PVN of Male and Female MC4R-HA$^{+/-}$ Mice Returned to Normal Weight after DIO, Expression of MC4R in Sim1/MC4R Neurons Is Recovered, whereas Loss of Non-Sim1/MC4R Neurons Persists

DIO decreases α-MSH protein abundance in POMC neurons of arcuate nucleus in male mice (Nyamugenda et al., 2019; Schneeberger et al., 2013; Thaler et al., 2012). Here, we find that male MC4R-HA mice with DIO also have decreased α-MSH abundance as compared with that of mice kept on LFD (by 31.00 ± 20.32%, $p < 0.05$), Figure 1A. Conversely, when the diet of male MC4R-HA $^{+/-}$ mice with DIO was switched from HF to LF, abundance of α-MSH in the arcuate nucleus was restored. Data indicate that, in MC4R-HA mice with DIO, injury to POMC neurons recovers upon switching diet from HF to LF. We have found that DIO induces loss of PVN neurons (Figure 1), but changing feeding from HF to LFD resumes neurogenesis (Figure 7). Here we asked whether, upon restoration of normal weight by dietary intervention, resumed neurogenesis would replace lost PVN neurons. Hypothalamic sections derived from male and female MC4R-HA $^{+/-}$ mice treated as in Figure 6A were stained with antibodies against the mature neuronal marker NeuN. The number of NeuN-positive cells in the PVN of male and female mice that were switched from HF to LFD remained decreased by 56.3 ± 19.5%, $p < 0.01$ and by 61.7 ± 30.2%, $p < 0.01$, respectively, as compared with that of mice kept on LFD for the entire duration of the study (Figures 8B and 8D). Thus, resumed neurogenesis upon dietary intervention is insufficient to reconstitute the normal population of PVN neurons in mice that returned to normal weight after DIO. DIO induces, rather than loss of Sim1/MC4R neurons, loss of MC4R protein (Figures 1 and 5). In the PVN of male and female MC4R-HA $^{+/-}$ mice that returned to normal weight after DIO, abundance of MC4R-HA protein was the same as that of lean mice fed with LFD for the entire duration of the study (Figures 8C and 8E). Thus, when mice with DIO return to normal weight, existing Sim1/MC4R neurons recover, thereby re-gaining the ability to express MC4R at the same level as mice never exposed to HF feeding.

DISCUSSION

The work described here finds that, in male and female mice with DIO, Sim1/MC4R neurons of the PVN have decreased abundance of MC4R but are nevertheless able to survive and recover MC4R expression when

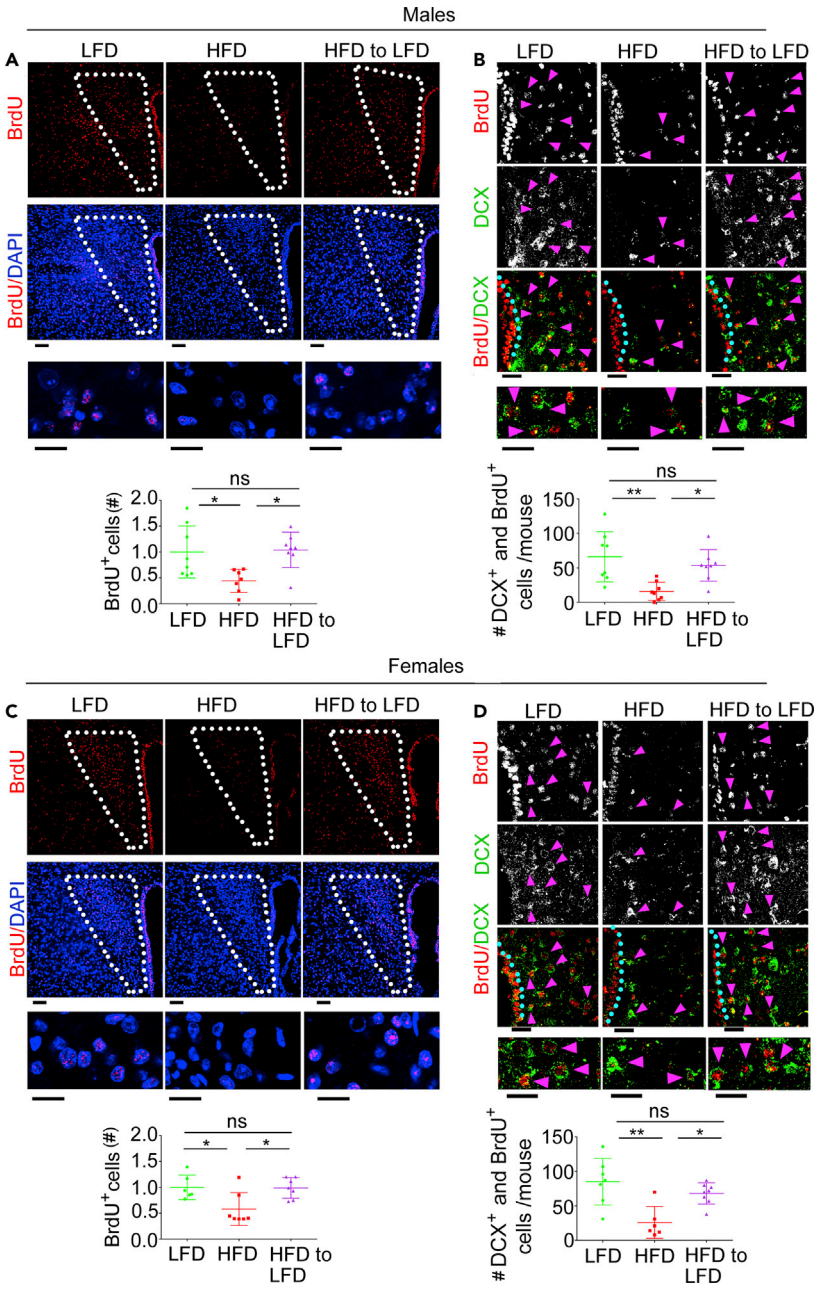

Figure 7. In the PVN of Male and Female MC4R-HA$^{+/-}$ Mice Returned to Normal Weight After DIO, Neurogenesis Is Restored

(A–D) Confocal microscopy of PVN sections of male and female MC4R-HA$^{+/-}$ mice treated with LFD, HFD, and HFD to LFD. (A and C) PVN sections are immunostained with anti-BrdU and co-stained with DAPI, males LFD, n = 8; HFD, n = 7; HFD to LFD n = 8; females, LFD, n = 6; HFD, n = 7; HFD to LFD n = 7; number of cells with nuclear BrdU is derived from two MIP images per mouse; scale bars: upper, 60 μm; lower, 8 μm. (B and D) PVN sections are immunostained with anti-BrdU and anti-DCX, males LFD, n = 8; HFD, n = 8; HFD to LFD n = 8; females, LFD, n = 7; HFD, n = 6; HFD to LFD n = 8; number of DCX and nuclear BrdU-positive cells are derived from eight confocal images per mouse taken along the third ventricle (3V) with the 60× objective; scale bars: upper, 30 μm; lower, 16 μm. *p < 0.05, **p < 0.01. Data are represented as mean values +/- SEM.

normal weight is restored by dietary intervention. Differently, DIO decreases the number of non-Sim1/MC4R neurons in the PVN. When mice with DIO return to normal weight, neurogenesis resumes in the PVN but is insufficient to replace the non-Sim1/MC4R neurons that were lost because of DIO. These

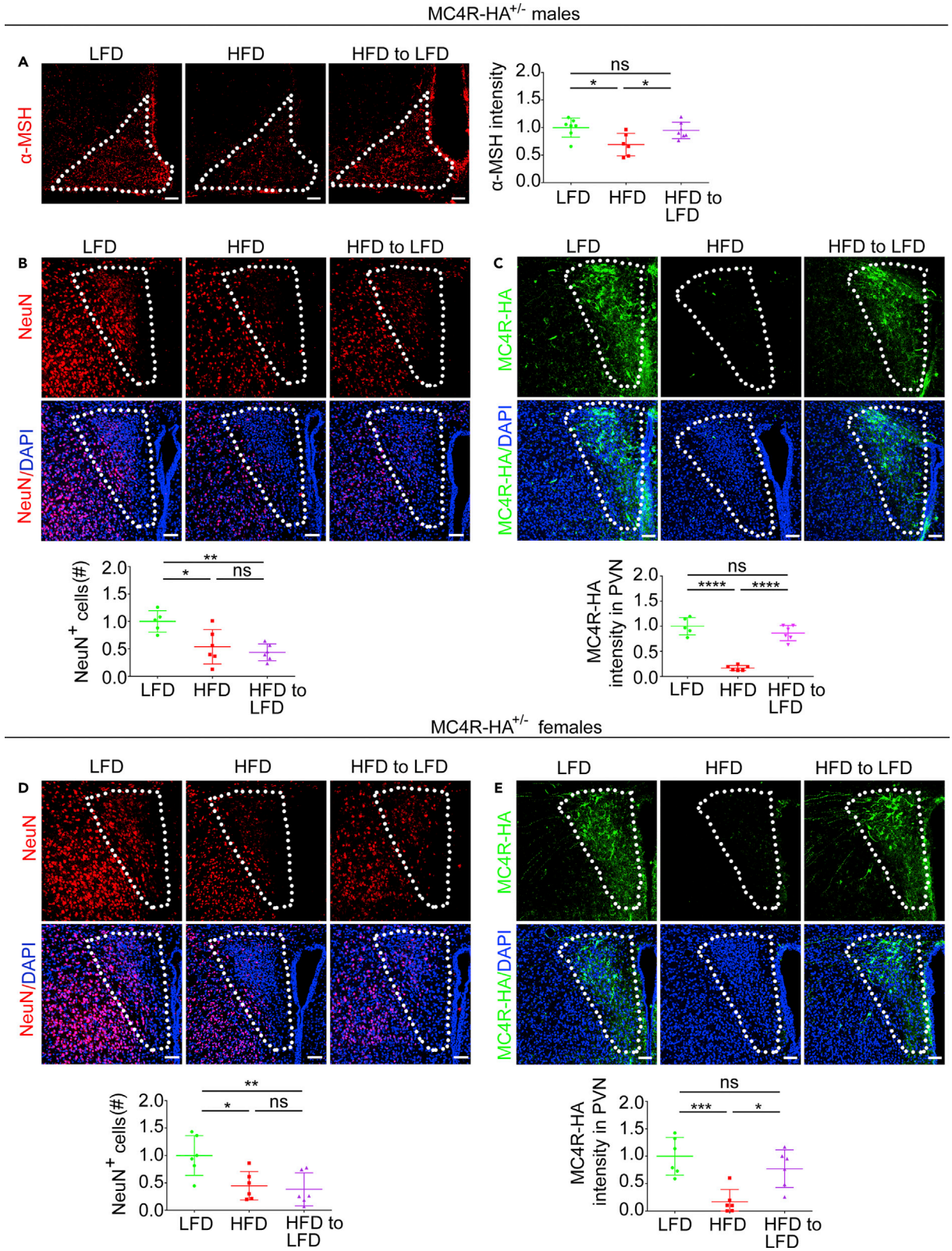
MC4R-HA+/- males
A
LFD
HFD
HFD to LFD
α-MSH
α-MSH intensity
ns
*
*
2.0
1.5
1.0
0.5
0.0
LFD
HFD
HFD to LFD
B
NeuN
NeuN/DAPI
NeuN+ cells (#)
**
*
ns
C
MC4R-HA
MC4R-HA/DAPI
MC4R-HA intensity in PVN
****
****
MC4R-HA+/- females
D
E
***

Figure 8. In Male and Female MC4R-HA$^{+/-}$ Mice Returned to Normal Weight after DIO, Expression of MC4R in Sim1/MC4R Neurons Is Recovered, Whereas Loss of Other PVN Neurons Persists

(A) Arcuate nucleus sections of male mice treated with LFD (n = 7), HFD (n = 6), and HFD to LFD (n = 7) are immunostained with anti-α-MSH.
(B–E) Confocal microscopy of PVN sections of male and female MC4R-HA$^{+/-}$ mice treated with LFD, HFD, and HFD to LFD. (B and D) PVN sections are immunostained with anti-NeuN and co-stained with DAPI, males LFD, n = 5; HFD, n = 6; HFD to LFD n = 6; females, LFD, n = 6; HFD, n = 6; HFD to LFD n = 6. (C and E) PVN sections are immunostained with anti-HA and co-stained with DAPI, males LFD, n = 5; HFD, n = 6; HFD to LFD n = 6; females, LFD, n = 6; HFD, n = 6; HFD to LFD n = 6. Data in graphs are normalized and derived from two MIP images per mouse. Scale bars, 60 μm. *p < 0.05, **p < 0.01, ***p < 0.001; ****, p < 0.0001. Data are represented as mean values +/- SEM.

data suggest that obesity, even when reversed, may have a long-term effect of reducing the population of PVN neurons. Data suggest that selective survival of MC4R neurons makes them a preferential target to restore energy homeostasis and to prevent recurrence of obesity.

Mapping sites and mechanisms of hypothalamic injury taking place in mice and humans with obesity is considered essential to understand the current epidemic of the disease. We have previously found that HFD induces apoptosis and neuronal loss in the PVN (Nyamugenda et al., 2019). However, it is not known whether such loss of PVN neurons extends to the population of PVN Sim1/MC4R neurons. Sapphire mice express GFP under the MC4R promoter, allowing for the identification of these neurons by immunofluorescence microscopy (Liu et al., 2003). We find here that GFP expression by the Sim1/MC4R neurons is not affected by exposure to HFD. With this respect, lipid stress appears to have a milder outcome on abundance of GFP, which folds in the cytosol, rather than on MC4R, which folds in the ER. Thus, because the detection system to monitor Sim1/MC4R neurons of the PVN remains unaltered in DIO, Sapphire mice appear a useful model to monitor survival of these neurons. By counting the number of GFP-expressing cells in the PVN, we find that exposure to HFD does not reduce the number of Sim1/MC4R neurons. These data indicate that, within the PVN, at least the population of Sim1/MC4R neurons that expresses GFP survives, thereby indicating selectivity in neuronal injury by HFD exposure. Analysis of MC4R abundance has not yet been carried out in the murine hypothalamus with DIO, likely because of lack of antibodies to reliably detect endogenous MC4R at this location. In knockin mice expressing MC4R-GFP with the GFP tag at the C terminus, the tagged receptor could not be visualized in the PVN at low magnification (Siljee et al., 2018). Nevertheless, low-magnification microscopy is a useful tool to determine the distribution and abundance of proteins in brain. We have here generated novel knockin MC4R-HA$^{+/-}$ mice, which express MC4R-HA with the small HA tag placed at the C terminus of the receptor. In these mice, MC4R-HA can be readily detected by using enzyme-linked immunofluorescence microscopy in Sim1/MC4R neurons of the PVN identified by genetically encoded GFP and mEGFP reporters expressed under the control of MC4R and Sim1 promoter, respectively (Balthasar et al., 2005; Liu et al., 2003; Panaro et al., 2014). When tested in neuronal cells, epitope-tagged MC4R-HA is able to generate cAMP with a similar EC_{50} as the WT MC4R and is thereby a functional receptor. In neuronal cells MC4R-HA has a predominant localization to clathrin-coated vesicles, similar to that of MC4R with the GFP tag at the C terminus. These data are consistent with MC4R being endocytosed (Mohammad et al., 2007), a process that appears to take place irrespective of the receptor being tagged with HA or with GFP. Post-synaptic localization of endogenous MC4R has been reported to take place at synaptic spines of hippocampal neurons in primary culture, where existing antibodies can detect the receptor (Shen et al., 2013). However, in the PVN, sites of α-MSH and AGRP release are predominantly at non-synaptic boutons of axons that extend from POMC neurons and AgRP neurons, respectively (Atasoy et al., 2014). In addition to predominantly peptidergic release sites, axons of POMC neurons reaching the PVN have sites of neurotransmitters release at classical neurotransmitter excitatory synapses that have also few peptide-containing vesicles and connect to dendrites (Atasoy et al., 2014). In addition to POMC neurons, fast-acting glutamatergic neurons that reside in the arcuate nucleus project from arcuate nucleus to the PVN to decrease appetite (Andermann and Lowell, 2017; Fenselau et al., 2017). We find here that, in the brain of mice co-expressing MC4R-HA and mEGFP in the Sim1/MC4R neurons, neuronal processes extend both within the PVN and outside of the PVN. The longer neuronal processes from Sim1/MC4R neurons that travel from PVN through regions lateral to PVN appear morphologically as axons and have sites of MC4R expression. In Sim1/MC4R neurons, a fraction of tagged MC4R-HA co-localizes with the post-synaptic marker PSD95. When placed in primary hypothalamic cultures, Sim1 neurons identified by the genetically encoded reporter mEGFP extend one long process, thereby morphologically identified as an axon that has sites of PSD95 accumulation along its entire length. PSD95 is expressed in virtually all brain excitatory glutamatergic synapses (Beique et al., 2006). Together, these observations suggest that a fraction of cell MC4R is localized to post-synaptic sites of excitatory synapses, which may exist along axons of Sim1/MC4R neurons that exit the PVN. Further work is required

to determine which population of neurons establishes contacts with the Sim1-MC4R neurons at these sites. It has also been found that tagged MC4R-GFP localizes to primary cilia in a subset of hypothalamus neurons (Siljee et al., 2018). Together, these data indicate multiple cell localization of MC4R that include post-synaptic site and primary cilia, perhaps to convey different types of signals in response to agonist release.

MC4R-HA$^{+/-}$ mice, similar to WT mice, increase their caloric intake and become obese when exposed to HFD and decrease caloric intake and return to normal weight upon dietary intervention, namely, replacing HFD with LFD (Berkseth et al., 2014; Enriori et al., 2007). POMC precursor is synthesized in the ER and processed to generate α-MSH in POMC neurons. DIO decreases α-MSH protein abundance in POMC neurons of the arcuate nucleus of male mice (Cakir et al., 2013; Nyamugenda et al., 2019; Schneeberger et al., 2013, 2015; Thaler et al., 2012). Conversely, male mice with DIO that have returned to normal weight by dietary intervention have restored leptin sensitivity in POMC neurons (Enriori et al., 2007). Consistent with these observations, we find here that MC4R-HA mice with DIO have decreased α-MSH and, upon returning to normal weight, restored abundance of α-MSH in arcuate nucleus. Therefore, MC4R-HA$^{+/-}$ mice mirror effects of HFD delivery and withdrawal taking place in WT rodents. MC4R-HA$^{+/-}$ mice appear as reliable models to study whether DIO and recovery from DIO modulate expression of MC4R in PVN neurons. By using MC4R-HA$^{+/-}$ mice, we find that DIO induces profound loss of MC4R abundance specific to the PVN. Importantly, MC4R-HA$^{+/-}$ mice that have returned to normal weight by decreasing their caloric intake after DIO have restored abundance of MC4R in the PVN. In male mice, the loss of α-MSH in POMC neurons, together with the decrease in MC4R abundance in the PVN described here, might cooperate to disrupt function of the melanocortin pathway, thereby promoting hyperphagia and obesity. However, under the same HFD conditions as male mice, female mice do not have decreased abundance of α-MSH (Nyamugenda et al., 2019 and Figure 1) but do have a reduced level of MC4R in the PVN and develop hyperphagia and obesity. MC4R in PVN is essential to control food intake and energy homeostasis (Balthasar et al., 2005). These data suggest loss of MC4R as a predominant factor to promote increased caloric intake and obesity in female mice fed HFD. Glutamatergic Sim1/MC4R neurons project from the PVN to the parabrachial nucleus to regulate appetite (Shah et al., 2014). Whether the population of PVN Sim1/MC4R neurons projecting to the parabrachial nucleus is the same as that found here to have decreased MC4R abundance upon exposure to HFD remains to be established. It has been reported that, in the PVN, Sim1/prodynorphin-expressing neurons, which do not express MC4R, function independently and additively with the Sim1/MC4R neurons to regulate appetite by projecting to the locus coeruleus (Li et al., 2019). Whether the population of Sim1/prodynorphin-expressing neurons of the PVN neurons is injured by exposure to HFD and whether it can recover when mice return to normal weight after DIO also remains to be established.

In DIO, MC4R signaling within the melanocortin pathway becomes over-responsive to α-MSH (Hansen et al., 2001) and to the synthetic MC4R agonist MTII (Cooney et al., 2017; Enriori et al., 2007). A prominent feature of obesity is increased circulating saturated fatty acid with changes in brain lipids and increased liver fat (Nam et al., 2017; Rosqvist et al., 2014; Valdearcos et al., 2014). Chronic exposure to MTII induces profound loss of MC4R signaling in neuronal cells (Molden et al., 2015). We have modeled *in vitro* hypothalamic injury due to exposure to excess saturated fat by incubating immortalized hypothalamic neurons and neuronal cells with elevated palmitate. Under these conditions, lipid stress induces loss of MC4R abundance and decreases acute MC4R response to agonist (Cooney et al., 2017; Cragle and Baldini, 2014). Importantly, neuronal cells and immortalized hypothalamic neurons exposed to elevated palmitate have also impaired clathrin-dependent endocytosis of MC4R, thereby resulting in inhibition of MC4R desensitization both in response to α-MSH and to MTII (Cooney et al., 2017). Thus, in DIO, blunted receptor desensitization may explain why mice with decreased abundance of MC4R are hypersensitive to agonists.

A feature of neurodegenerative diseases, such as Alzheimer's and Parkinson's diseases, is disrupted mitochondrial function with defects in the function of Cox, the terminal enzyme complex of the respiratory chain (Arnold, 2012; Schull et al., 2015; Timper and Bruning, 2017; Van der Schueren et al., 2015). Mitochondrial dysfunction in POMC neurons of the arcuate nucleus is also a prominent hypothalamic feature of obesity (Quarta et al., 2019; Schneeberger et al., 2013; Toda et al., 2017). In the hypothalamus of mice with DIO, increased level of saturated fat induces inflammatory signaling in the microglia, which promotes mitochondrial dysfunction in POMC neurons residing in the arcuate nucleus (Kim et al., 2019; Paeger et al., 2017; Valdearcos et al., 2014, 2017; Yi et al., 2017). We find that DIO induces in the Sim1/MC4R neurons of the PVN identified by genetically encoded GFP decreased cell content of CoxIV, thereby indicating mitochondrial

injury. However, and differently than in the mediobasal hypothalamus, proliferation and activation of microglia does not take place in PVN (Nyamugenda et al., 2019). On the other hand, we find here that direct exposure of neuronal Neuro2A cells to elevated palmitate is sufficient to decrease cell content of CoxIV, thereby mirroring mitochondrial injury by DIO in the Sim1/MC4R neurons. CoxIV contributes to the formation of proton electrochemical gradient across the inner mitochondrial membrane (Breuer et al., 2013). In this respect, we find here that exposure to elevated palmitate induces in primary hypothalamic neurons, together with the loss of cell CoxIV, also a decrease of overall cell mitochondrial membrane potential. These findings suggest that increased level of saturated fat in the hypothalamus of mice with DIO (Valdearcos et al., 2014) causes injury to the mitochondria of Sim1/MC4R neurons by a direct mechanism. Super-resolution microscopy allows detection of morphological mitochondrial changes in a large population of Sim1/MC4R neurons. By using this approach, we find here that, in addition to loss of cell COXIV abundance, there is also loss of cell mitochondria content and reduced extension of mitochondrial network. Together, these data indicate that, in DIO, Sim1/MC4R neurons have profound mitochondrial injury, which appears to be, at least in part, a direct consequence of exposure to excess saturated fat.

Because Sim1/MC4R neurons are damaged by exposure to HFD, we asked whether selective persistence of these neurons under DIO is due to their ability to regenerate and to replace lost neurons. Hypothalamic neuronal regeneration takes place from proliferating tancytes localized to the ependymal layer next to the third ventricle (Robins et al., 2013; Yoo and Blackshaw, 2018). We find here that intraperitoneal delivery of BrdU at low dose for 1 week labels predominantly cells in the ependymal layer, consistent with this region being the niche of hypothalamic neurogenesis. We also find that BrdU-labeled cells are present in the PVN and that 15%–20% of the population of Sim1/MC4R neurons originates from cells that proliferated during the 1-week interval of BrdU delivery. These data suggest that, in healthy adult rodents, there is continuous basal renewal of Sim1/MC4R neurons. In DIO, regeneration of Sim1/MC4R neurons almost halts in the PVN of male mice. However, in male mice under HF feeding conditions, the size of the Sim1/MC4R neuronal population remains unchanged. Thus, under HF feeding, existing Sim1/MC4R neurons may persist for a longer time than those of male mice under LF feeding. In male mice with DIO, the drop in caloric intake takes place already in the first week after switching diet from HF to LF. Data suggest that, upon dietary intervention, recovered abundance of MC4R takes place immediately in already existing Sim1/MC4R and controls caloric intake. Consistent with this possibility, MC4R abundance appears fully restored 4 weeks after dietary intervention. Conversely, neurogenesis of Sim1/MC4R neurons continues in female mice exposed to HFD. Thus, it is possible that, in female mice with DIO, switching diet from HF to LF recovers control of caloric intake by a combination of factors, namely, Sim1/MC4R neuronal regeneration together with recovered MC4R expression in existing Sim1/MC4R neurons. Here, we also find that, in male and female mice with DIO, switch from HF to LFD prompts re-appearance of DCX- and BrdU-positive cells in PVN to the same level as that of mice treated with LFD. These data indicate that rodent PVN neurons can resume neurogenesis from proliferating cells after DIO. Nevertheless, DIO decreases the general population of non-Sim1/MC4R PVN neurons in male and female mice, as shown here and reported previously (Nyamugenda et al., 2019). Moreover, neurogenesis after DIO does not repopulate the population of lost non-Sim1 PVN neurons when normal weight is re-gained. The concept that neurogenesis can take place in the adult human brain has recently been put into question (Snyder, 2018; Sorrells et al., 2018). In light of this, and together with the data presented here indicating selective survival of Sim1/MC4R neurons in DIO and ability to recover MC4R expression, these neurons present a preferential target of therapy to promote weight loss and prevent recurrence of obesity.

Limitations of the Study

We did not identify which population(s) of non-Sim1/MC4R PVN neurons is lost upon exposure of mice to HFD. Further studies are required to identify these neurons. We did not determine whether the population of PVN Sim1/MC4R neurons that have decreased MC4R upon exposure to HFD includes the one that regulates feeding and projects to the parabrachial nucleus. Further studies are required to determine whether this is the case.

Resource Availability

Lead Contact

Further information and requests for resources and reagents should be directed to and will be fulfilled by the Lead Contact, Giulia Baldini (GBaldini@uams.edu).

Materials Availability

There are restrictions to the availability of mice and other reagents owing to the lack of an external centralized repository for their distribution and our need to maintain the stock. We are glad to share mice and other reagents with reasonable compensation by requestor for their processing and shipping. Unique/stable reagents generated in this study are available from the Lead Contact with a completed Materials Transfer Agreement.

Data and Code Availability

This study did not generate/analyze datasets/code.

METHODS

All methods can be found in the accompanying Transparent Methods supplemental file.

SUPPLEMENTAL INFORMATION

Supplemental Information can be found online at https://doi.org/10.1016/j.isci.2020.101114.

ACKNOWLEDGMENTS

This work was supported by National Institutes of Health Grants R01-DK102206 (to G.B.), by UL1TR000039, by NIGMS Grant 5R25GM083247-0 (UAMS IMSD), and by Intramural Funding Support from the University of Arkansas for Medical Sciences College of Medicine and by P20GM125503 (COBRE, Center for Musculoskeletal Disease Research [CMDR], Director, Charles O'Brien). We thank Charles O'Brien and Joseph Goellner for help generating the MC4R-HA$^{+/-}$ mice.

AUTHOR CONTRIBUTIONS

Conceptualization, G.B. and K.D.P.; Methodology E.N., S.R., G.B., and K.D.P.; Investigation, E.N., H.G., S.R., K.C., N.S.K., I.I., K.D.P., G.B.; Writing – Original Draft, E.N., G.B., and K.D.P.; Writing – Review & Editing, E.N., G.B., and K.D.P.; Funding Acquisition, G.B. and K.D.P.; Supervision, S.R., G.B., and K.D.P.

DECLARATION OF INTERESTS

Authors do not have any competing interests.

Received: February 10, 2020
Revised: March 19, 2020
Accepted: April 27, 2020
Published: May 22, 2020

REFERENCES

Andermann, M.L., and Lowell, B.B. (2017). Toward a wiring diagram understanding of appetite control. Neuron *95*, 757–778.

Arnold, S. (2012). Cytochrome c oxidase and its role in neurodegeneration and neuroprotection. Adv. Exp. Med. Biol. *748*, 305–339.

Atasoy, D., Betley, J.N., Li, W.P., Su, H.H., Sertel, S.M., Scheffer, L.K., Simpson, J.H., Fetter, R.D., and Sternson, S.M. (2014). A genetically specified connectomics approach applied to long-range feeding regulatory circuits. Nat. Neurosci. *17*, 1830–1839.

Ayanlaja, A.A., Xiong, Y., Gao, Y., Ji, G., Tang, C., Abdikani Abdullah, Z., and Gao, D. (2017). Distinct features of doublecortin as a marker of neuronal migration and its implications in cancer cell mobility. Front. Mol. Neurosci. *10*, 199.

Bach, D., Pich, S., Soriano, F.X., Vega, N., Baumgartner, B., Oriola, J., Daugaard, J.R., Lloberas, J., Camps, M., Zierath, J.R., et al. (2003). Mitofusin-2 determines mitochondrial network architecture and mitochondrial metabolism. A novel regulatory mechanism altered in obesity. J. Biol. Chem. *278*, 17190–17197.

Baldini, G., and Phelan, K.D. (2019). The melanocortin pathway and control of appetite-progress and therapeutic implications. J. Endocrinol. *241*, R1–R33.

Balthasar, N., Dalgaard, L.T., Lee, C.E., Yu, J., Funahashi, H., Williams, T., Ferreira, M., Tang, V., McGovern, R.A., Kenny, C.D., et al. (2005). Divergence of melanocortin pathways in the control of food intake and energy expenditure. Cell *123*, 493–505.

Batailler, M., Droguerre, M., Baroncini, M., Fontaine, C., Prevot, V., and Migaud, M. (2014). DCX-expressing cells in the vicinity of the hypothalamic neurogenic niche: a comparative study between mouse, sheep, and human tissues. J. Comp. Neurol. *522*, 1966–1985.

Beique, J.C., Lin, D.T., Kang, M.G., Aizawa, H., Takamiya, K., and Huganir, R.L. (2006). Synapse-specific regulation of AMPA receptor function by PSD-95. Proc. Natl. Acad. Sci. U S A *103*, 19535–19540.

Berkseth, K.E., Guyenet, S.J., Melhorn, S.J., Lee, D., Thaler, J.P., Schur, E.A., and Schwartz, M.W. (2014). Hypothalamic gliosis associated with high-fat diet feeding is reversible in mice: a combined immunohistochemical and magnetic resonance imaging study. Endocrinology *155*, 2858–2867.

Breuer, M.E., Koopman, W.J., Koene, S., Nooteboom, M., Rodenburg, R.J., Willems, P.H., and Smeitink, J.A. (2013). The role of mitochondrial OXPHOS dysfunction in the development of neurologic diseases. Neurobiol. Dis. *51*, 27–34.

Brown, J.P., Couillard-Despres, S., Cooper-Kuhn, C.M., Winkler, J., Aigner, L., and Kuhn, H.G. (2003). Transient expression of doublecortin during adult neurogenesis. J. Comp. Neurol. *467*, 1–10.

Cakir, I., Cyr, N.E., Perello, M., Litvinov, B.P., Romero, A., Stuart, R.C., and Nillni, E.A. (2013). Obesity induces hypothalamic endoplasmic reticulum stress and impairs proopiomelanocortin (POMC) post-translational processing. J. Biol. Chem. *288*, 17675–17688.

Cooney, K.A., Molden, B.M., Kowalczyk, N.S., Russell, S., and Baldini, G. (2017). Lipid stress inhibits endocytosis of melanocortin-4 receptor from modified clathrin-enriched sites and impairs receptor desensitization. J. Biol. Chem. *292*, 17731–17745.

Cragle, F.K., and Baldini, G. (2014). Mild lipid stress induces profound loss of MC4R protein abundance and function. Mol. Endocrinol. *28*, 357–367.

De Souza, C.T., Araujo, E.P., Bordin, S., Ashimine, R., Zollner, R.L., Boschero, A.C., Saad, M.J.A., and Velloso, L.A. (2005). Consumption of a fat-rich diet activates a proinflammatory response and induces insulin resistance in the hypothalamus. Endocrinology *146*, 4192–4199.

Dorfman, M.D., Krull, J.E., Douglass, J.D., Fasnacht, R., Lara-Lince, F., Meek, T.H., Shi, X., Damian, V., Nguyen, H.T., Matsen, M.E., et al. (2017). Sex differences in microglial CX3CR1 signalling determine obesity susceptibility in mice. Nat. Commun. *8*, 14556.

Dorfman, M.D., and Thaler, J.P. (2015). Hypothalamic inflammation and gliosis in obesity. Curr. Opin. Endocrinol. Diabetes Obes. *22*, 325–330.

Enriori, P.J., Evans, A.E., Sinnayah, P., Jobst, E.E., Tonelli-Lemos, L., Billes, S.K., Glavas, M.M., Grayson, B.E., Perello, M., Nillni, E.A., et al. (2007). Diet-induced obesity causes severe but reversible leptin resistance in arcuate melanocortin neurons. Cell Metab. *5*, 181–194.

Fenselau, H., Campbell, J.N., Verstegen, A.M., Madara, J.C., Xu, J., Shah, B.P., Resch, J.M., Yang, Z., Mandelblat-Cerf, Y., Livneh, Y., et al. (2017). A rapidly acting glutamatergic ARC–>PVH satiety circuit postsynaptically regulated by alpha-MSH. Nat. Neurosci. *20*, 42–51.

Hansen, M.J., Ball, M.J., and Morris, M.J. (2001). Enhanced inhibitory feeding response to alpha-melanocyte stimulating hormone in the diet-induced obese rat. Brain Res. *892*, 130–137.

Horvath, T.L., Sarman, B., Garcia-Caceres, C., Enriori, P.J., Sotonyi, P., Shanabrough, M., Borok, E., Argente, J., Chowen, J.A., Perez-Tilve, D., et al. (2010). Synaptic input organization of the melanocortin system predicts diet-induced hypothalamic reactive gliosis and obesity. Proc. Natl. Acad. Sci. U S A *107*, 14875–14880.

Kim, J.D., Yoon, N.A., Jin, S., and Diano, S. (2019). Microglial UCP2 mediates inflammation and obesity induced by high-fat feeding. Cell Metab. *30*, 952–962.e5.

Klockener, T., Hess, S., Belgardt, B.F., Paeger, L., Verhagen, L.A., Husch, A., Sohn, J.W., Hampel, B., Dhillon, H., Zigman, J.M., et al. (2011). High-fat feeding promotes obesity via insulin receptor/PI3K-dependent inhibition of SF-1 VMH neurons. Nat. Neurosci. *14*, 911–918.

Kokoeva, M.V., Yin, H., and Flier, J.S. (2005). Neurogenesis in the hypothalamus of adult mice: potential role in energy balance. Science *310*, 679–683.

Li, J., Tang, Y., and Cai, D. (2012). IKKbeta/NF-kappaB disrupts adult hypothalamic neural stem cells to mediate a neurodegenerative mechanism of dietary obesity and pre-diabetes. Nat. Cell Biol. *14*, 999–1012.

Li, M.M., Madara, J.C., Steger, J.S., Krashes, M.J., Balthasar, N., Campbell, J.N., Resch, J.M., Conley, N.J., Garfield, A.S., and Lowell, B.B. (2019). The paraventricular hypothalamus regulates satiety and prevents obesity via two genetically distinct circuits. Neuron *102*, 653–667.e6.

Liu, H., Kishi, T., Roseberry, A.G., Cai, X., Lee, C.E., Montez, J.M., Friedman, J.M., and Elmquist, J.K. (2003). Transgenic mice expressing green fluorescent protein under the control of the melanocortin-4 receptor promoter. J. Neurosci. *23*, 7143–7154.

Matsuzaki, K., Katakura, M., Inoue, T., Hara, T., Hashimoto, M., and Shido, O. (2015). Aging attenuates acquired heat tolerance and hypothalamic neurogenesis in rats. J. Comp. Neurol. *523*, 1190–1201.

McNay, D.E.G., Briancon, N., Kokoeva, M.V., Maratos-Flier, E., and Flier, J.S. (2012). Remodeling of the arcuate nucleus energy-balance circuit is inhibited in obese mice. J. Clin. Invest. *122*, 142–152.

Mohammad, S., Baldini, G., Granell, S., Narducci, P., Martelli, A.M., and Baldini, G. (2007). Constitutive traffic of melanocortin-4 receptor in Neuro2A cells and immortalized hypothalamic neurons. J. Biol. Chem. *282*, 4963–4974.

Molden, B.M., Cooney, K.A., West, K., Van Der Ploeg, L.H., and Baldini, G. (2015). Temporal cAMP signaling selectivity by natural and synthetic MC4R agonists. Mol. Endocrinol. *29*, 1619–1633.

Nam, K.N., Mounier, A., Wolfe, C.M., Fitz, N.F., Carter, A.Y., Castranio, E.L., Kamboh, H.I., Reeves, V.L., Wang, J., Han, X., et al. (2017). Effect of high fat diet on phenotype, brain transcriptome and lipidome in Alzheimer's model mice. Sci. Rep. *7*, 4307.

Nyamugenda, E., Trentzsch, M., Russell, S., Miles, T., Boysen, G., Phelan, K.D., and Baldini, G. (2019). Injury to hypothalamic Sim1 neurons is a common feature of obesity by exposure to high-fat diet in male and female mice. J. Neurochem. *149*, 73–97.

Paeger, L., Pippow, A., Hess, S., Paehler, M., Klein, A.C., Husch, A., Pouzat, C., Bruning, J.C., and Kloppenburg, P. (2017). Energy imbalance alters Ca(2+) handling and excitability of POMC neurons. Elife *6*, e25641.

Panaro, B.L., Tough, I.R., Engelstoft, M.S., Matthews, R.T., Digby, G.J., Moller, C.L., Svendsen, B., Gribble, F., Reimann, F., Holst, J.J., et al. (2014). The melanocortin-4 receptor is expressed in enteroendocrine L cells and regulates the release of peptide YY and glucagon-like peptide 1 in vivo. Cell Metab. *20*, 1018–1029.

Qiu, J., Bosch, M.A., Meza, C., Navarro, U.V., Nestor, C.C., Wagner, E.J., Ronnekleiv, O.K., and Kelly, M.J. (2018). Estradiol protects proopiomelanocortin neurons against insulin resistance. Endocrinology *159*, 647–664.

Quarta, C., Fioramonti, X., and Cota, D. (2019). POMC neurons dysfunction in diet-induced metabolic disease: hallmark or mechanism of disease? Neuroscience, https://doi.org/10.1016/j.neuroscience.2019.09.031.

Robins, S.C., Stewart, I., McNay, D.E., Taylor, V., Giachino, C., Goetz, M., Ninkovic, J., Briancon, N., Maratos-Flier, E., Flier, J.S., et al. (2013). alpha-Tanycytes of the adult hypothalamic third ventricle include distinct populations of FGF-responsive neural progenitors. Nat. Commun. *4*, 2049.

Rosqvist, F., Iggman, D., Kullberg, J., Cedernaes, J., Johansson, H.E., Larsson, A., Johansson, L., Ahlstrom, H., Arner, P., Dahlman, I., et al. (2014). Overfeeding polyunsaturated and saturated fat causes distinct effects on liver and visceral fat accumulation in humans. Diabetes *63*, 2356–2368.

Schneeberger, M., Dietrich, M.O., Sebastian, D., Imbernon, M., Castano, C., Garcia, A., Esteban, Y., Gonzalez-Franquesa, A., Rodriguez, I.C., Bortolozzi, A., et al. (2013). Mitofusin 2 in POMC neurons connects ER stress with leptin resistance and energy imbalance. Cell *155*, 172–187.

Schneeberger, M., Gomez-Valades, A.G., Altirriba, J., Sebastian, D., Ramirez, S., Garcia, A., Esteban, Y., Drougard, A., Ferres-Coy, A., Bortolozzi, A., et al. (2015). Reduced alpha-MSH underlies hypothalamic ER-stress-induced hepatic gluconeogenesis. Cell Rep. *12*, 361–370.

Schull, S., Gunther, S.D., Brodesser, S., Seeger, J.M., Tosetti, B., Wiegmann, K., Pongratz, C., Diaz, F., Witt, A., Andree, M., et al. (2015). Cytochrome c oxidase deficiency accelerates mitochondrial apoptosis by activating ceramide synthase 6. Cell Death Dis. *6*, e1691.

Shah, B.P., Vong, L., Olson, D.P., Koda, S., Krashes, M.J., Ye, C., Yang, Z., Fuller, P.M., Elmquist, J.K., and Lowell, B.B. (2014). MC4R-expressing glutamatergic neurons in the paraventricular hypothalamus regulate feeding and are synaptically connected to the parabrachial nucleus. Proc. Natl. Acad. Sci. U S A *111*, 13193–13198.

Shen, Y., Fu, W.Y., Cheng, E.Y., Fu, A.K., and Ip, N.Y. (2013). Melanocortin-4 receptor regulates hippocampal synaptic plasticity through a protein kinase A-dependent mechanism. J. Neurosci. *33*, 464–472.

Siljee, J.E., Wang, Y., Bernard, A.A., Ersoy, B.A., Zhang, S., Marley, A., Von Zastrow, M., Reiter, J.F., and Vaisse, C. (2018). Subcellular localization of MC4R with ADCY3 at neuronal primary cilia underlies a common pathway for genetic predisposition to obesity. Nat. Genet. *50*, 180–185.

Smith, S.E., Granell, S., Salcedo-Sicilia, L., Baldini, G., Egea, G., and Teckman, J.H. (2011). Activating transcription factor 6 limits intracellular accumulation of mutant alpha(1)-antitrypsin Z and

mitochondrial damage in hepatoma cells. J. Biol. Chem. *286*, 41563–41577.

Snyder, J.S. (2018). Questioning human neurogenesis. Nature *555*, 315–316.

Sorrells, S.F., Paredes, M.F., Cebrian-Silla, A., Sandoval, K., Qi, D., Kelley, K.W., James, D., Mayer, S., Chang, J., Auguste, K.I., et al. (2018). Human hippocampal neurogenesis drops sharply in children to undetectable levels in adults. Nature *555*, 377–381.

Srinivasan, S., Santiago, P., Lubrano, C., Vaisse, C., and Conklin, B.R. (2007). Engineering the melanocortin-4 receptor to control constitutive and ligand-mediated G(S) signaling in vivo. PLoS One *2*, e668.

Thaler, J.P., Yi, C.X., Schur, E.A., Guyenet, S.J., Hwang, B.H., Dietrich, M.O., Zhao, X., Sarruf, D.A., Izgur, V., Maravilla, K.R., et al. (2012). Obesity is associated with hypothalamic injury in rodents and humans. J. Clin. Invest. *122*, 153–162.

Timper, K., and Bruning, J.C. (2017). Hypothalamic circuits regulating appetite and energy homeostasis: pathways to obesity. Dis. Model. Mech. *10*, 679–689.

Timper, K., Paeger, L., Sanchez-Lasheras, C., Varela, L., Jais, A., Nolte, H., Vogt, M.C., Hausen, A.C., Heilinger, C., Evers, N., et al. (2018). Mild impairment of mitochondrial OXPHOS promotes fatty acid utilization in POMC neurons and improves glucose homeostasis in obesity. Cell Rep *25*, 383–397.e10.

Toda, C., Santoro, A., Kim, J.D., and Diano, S. (2017). POMC neurons: from birth to death. Annu. Rev. Physiol. *79*, 209–236.

Trentzsch, M., Nyamugenda, E., Miles, T.K., Griffin, H., Russell, S., Koss, B., Cooney, K.A., Phelan, K.D., Tackett, A.J., Iyer, S., et al. (2020). Delivery of phosphatidylethanolamine blunts stress in hepatoma cells exposed to elevated palmitate by targeting the endoplasmic reticulum. Cell Death Discov. *6*, 8.

Valdearcos, M., Robblee, M.M., Benjamin, D.I., Nomura, D.K., Xu, A.W., and Koliwad, S.K. (2014). Microglia dictate the impact of saturated fat consumption on hypothalamic inflammation and neuronal function. Cell Rep. *9*, 2124–2138.

Valdearcos, M., Douglass, J.D., Robblee, M.M., Dorfman, M.D., Stifler, D.R., Bennett, M.L., Gerritse, I., Fasnacht, R., Barres, B.A., Thaler, J.P., et al. (2017). Microglial inflammatory signaling orchestrates the hypothalamic immune response to dietary excess and mediates obesity susceptibility. Cell Metab. *26*, 185–197.e3.

Van der Schueren, B., Vangoitsenhoven, R., Geeraert, B., De Keyzer, D., Hulsmans, M., Lannoo, M., Huber, H.J., Mathieu, C., and Holvoet, P. (2015). Low cytochrome oxidase 4I1 links mitochondrial dysfunction to obesity and type 2 diabetes in humans and mice. Int. J. Obes. (Lond) *39*, 1254–1263.

Velloso, L.A., Torsoni, M.A., and Araujo, E.P. (2009). Hypothalamic dysfunction in obesity. Rev. Neurosci. *20*, 441–449.

Xu, Y., Tamamaki, N., Noda, T., Kimura, K., Itokazu, Y., Matsumoto, N., Dezawa, M., and Ide, C. (2005). Neurogenesis in the ependymal layer of the adult rat 3rd ventricle. Exp. Neurol. *192*, 251–264.

Yi, C.X., Walter, M., Gao, Y., Pitra, S., Legutko, B., Kalin, S., Layritz, C., Garcia-Caceres, C., Bielohuby, M., Bidlingmaier, M., et al. (2017). TNFalpha drives mitochondrial stress in POMC neurons in obesity. Nat. Commun. *8*, 15143.

Yoo, S., and Blackshaw, S. (2018). Regulation and function of neurogenesis in the adult mammalian hypothalamus. Prog. Neurobiol. *170*, 53–66.

iScience, Volume *23*

Supplemental Information

Selective Survival of Sim1/MC4R Neurons in Diet-Induced Obesity

Eugene Nyamugenda, Haven Griffin, Susan Russell, Kimberly A. Cooney, Nicholas S. Kowalczyk, Ishrar Islam, Kevin D. Phelan, and Giulia Baldini

Supplementary Figures

Fig. S1

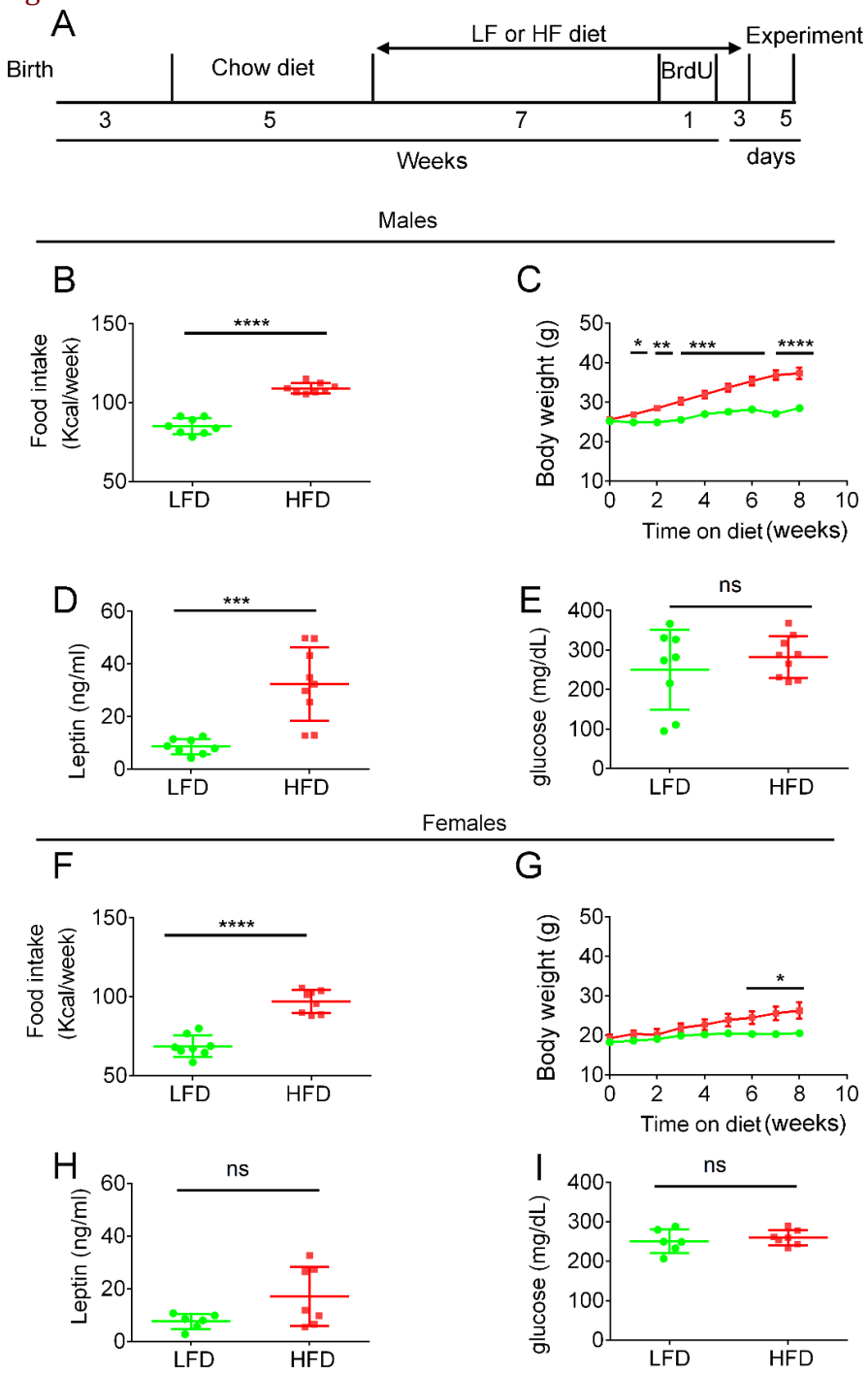

Figure S1. Related to Fig. 1. HF diet induces obesity in male and female Sapphire mice. (A) male and female 8-week-old mice were fed LF diet and high fat diet HF diet, respectively, for the following eight weeks. In the last week of diet treatment, all mice received one IP injection of BrdU, 50 mg/kg per day for seven days. (B-E) Weekly food intake per week, body weight, serum leptin, and blood glucose of male Sapphire mice treated with LFD, n = 8 and HFD, n = 9 mice. (F-I) Weekly food intake per week, weight, serum leptin, and blood glucose of female Sapphire mice treated with LFD, n = 6 and HFD diet, n = 7. * $p < 0.05$, ** $p < 0.01$, *** $p < 0.001$; ****, $p < 0.0001$. B, D, E, F, H and I, data are represented as mean values +/- SD. C and G, data are represented as mean values +/- standard error of the mean (SEM).

Supplementary Figures
Fig. S2

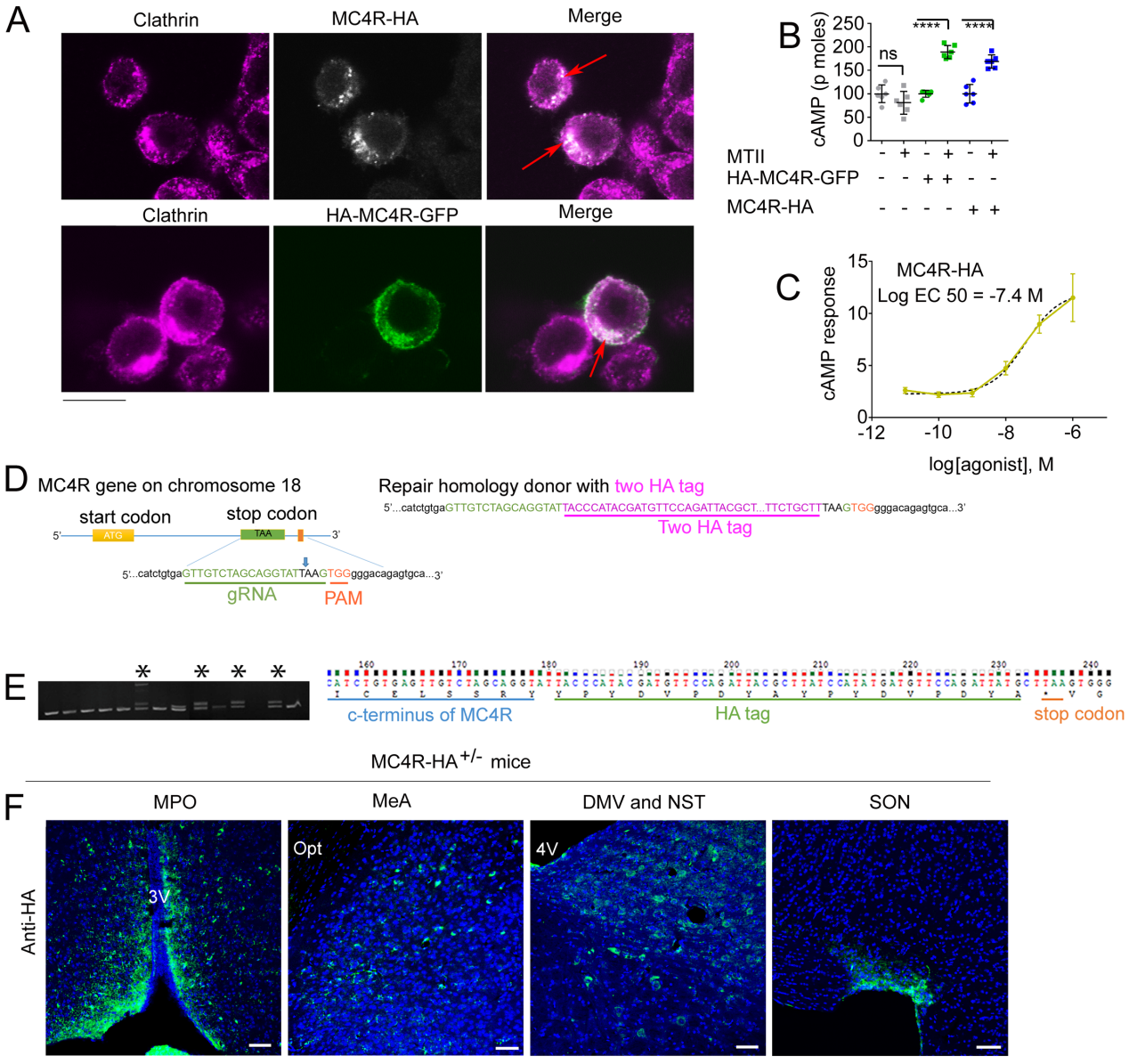

Figure S2. Related to Fig. 4. Knock-in MC4R-HA$^{+/-}$ mice express HA-tagged MC4R protein. (A) Confocal microscopy of Neuro2A cells expressing MC4R-HA and HA-MC4R-GFP immunostained with antibodies against HA and Clathrin. Red arrows indicate sites of MC4R-HA and HA-MC4R-GFP colocalization with clathrin. Scale bar, 10 μm. (B) Synthetic MC4R agonist, MTII, increases cAMP in Neuro2A cells expressing HA-MC4R-GFP and MC4R-HA, respectively. (C) Dose-response of MC4R-HA in Neuro2A cells. (D) Schematic of MC4R DNA coding region on chromosome 18 with guide RNA (gRNA) to target the 3' end of the MC4R gene and the repair homology donor with 2XHA tag (magenta). (E) DNA agarose gel analysis of MC4R PCR products. DNA from founder knock-in MC4R-HA mice has a higher molecular weight band due to insertion of 54 bp DNA encoding the 2XHA sequence (asterisks). Sequencing of the PCR products from founder mice indicates successful insertion of 2X HA sequence. (F) MC4R-HA is detectable in the medial preoptic area, MPO; Medial Amygdala, MeA; Dorsal Motor Nucleus of the Vagus, DMV; Nucleus of the Solitary Tract, NST; and Supraoptic Nucleus (SON) SON of the MC4R-HA$^{+/-}$ mouse. Scale bar, 60 μm.

Supplementary Figures
Fig. S3

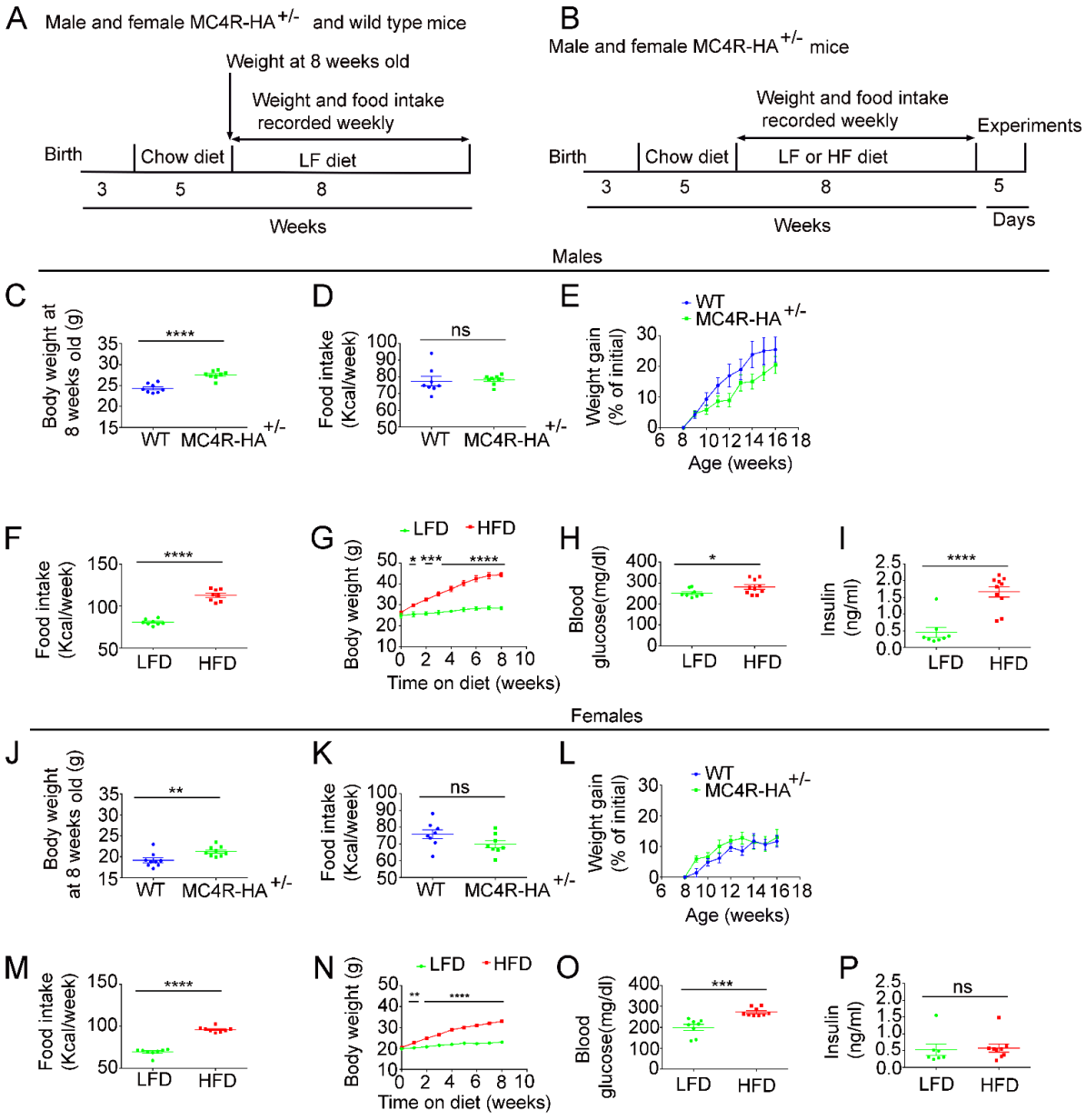

Figure S3. Related to Fig. 5. MC4R-HA$^{+/-}$ mice have similar weight gain and food intake as WT mice when fed a LF diet and develop obesity when exposed to HF diet. (A) Male and female 8 week-old wt and MC4R-HA$^{+/-}$ mice treated with LFD for 8 weeks. (B) Male and female MC4R-HA$^{+/-}$ mice treated with LFD and HFD diet, respectively for 8 weeks. (C-E) Body weight, food intake and weight gain of male WT mice (n= 8) and MC4R-HA$^{+/-}$ mice (n = 8) treated as in (A). (F-I) Food intake, bodyweight, blood glucose, and serum insulin of male MC4R-HA$^{+/-}$ mice treated as in B (LFD, n = 8 and HFD, n = 10). (J-L) Body weight, food intake and weight gain of female WT mice (n = 9) and MC4R-HA$^{+/-}$ mice (n = 9) treated as in (A). (M-P) Food intake, bodyweight, blood glucose, and serum insulin of female MC4R-HA$^{+/-}$ mice diet treated as in B (LFD, n = 7-9 and HFD, n = 9-10). * $p < 0.05$, ** $p < 0.01$, *** $p < 0.001$; ****, $p < 0.0001$. C, D, F ,H , I , J , K , M, O and P, data are represented as mean values +/- SD. E, G, L and N, data are represented as mean values +/- standard error of the mean (SEM).

Transparent Methods

Reagents

Capillary tubes for retro-orbital bleeding (Cat. # 22-260943), Optimal Cutting Temperature Compound (OTC, Cat. # 4585), formaldehyde (Cat. # BP531-500), Corning Penicillin/Streptomycin 50X (Cat. # MT30001CI), Standard High-Profile Disposable Blades (Cat. # 10-015-93) Corning® 100-1000 µL Universal Fit Racked Pipet Tips (Cat. # 07-200-304), AccuTec Blades™ Personna Single-edge Prep Razor Blades (Cat. # 12-640-18), Corning Falcon™ Cell Strainers (Cat. # 08-771-2) and Fisherbrand™ Superfrost™ Plus Microscope Slides (Cat. # 22-037-246) were purchased from Fisher Scientific. Neurobasal™-A Medium, no D-glucose, no sodium pyruvate, Cat. # A2477501, dithiothreitol (DTT, Cat. # R0861) and B-27™ Supplement (50X) serum free (Cat. # 17504044) MitoTracker™ Red CMXRos (MitoTracker, Cat. # M7512), and Hank's Balanced Salt Solution (HBSS, Cat. # 14170112) were purchased from ThermoFisher Scientific. Seahorse XF 100 mM pyruvate solution (Cat. # 103578-100) Seahorse XF 1.0 M glucose solution (Cat. # 103577-100) were from Agilent. 0.01% Poly-D-Lysine solution (Cat # 3439-100-01) was from R&D Systems. Fetal Bovine Serum (FBS) (Cat. # F-0500-A) was purchased from Atlas Biologicals. Papain (Cat. # LS0031191) and Earle's Balanced Salt Solution (EBSS, Cat. # LK003188) were purchased from Worthington Biochemical Corporation. Glass Bottom Culture Dishes/Plates was from Nest Scientific USA Inc. (Cat. # 801002). Ultra-Sensitive Mouse Insulin Enzyme-Linked Immunosorbent Assay (ELISA) Kit (Cat. # 90080) and Leptin ELISA Kit (Cat. # 90030) were from Crystal Chem. Nile Red (Cat. # N3013), bovine serum albumin (BSA) (Cat. # A7511-10G) and DNase I (Cat. #11284932001) were from Sigma-Aldrich. Heparin (Cat. # P87721) was purchased from Braun Medical. Click-it Terminal deoxynucleotidyl transferase Nick End Labeling (TUNEL) Assay kit (Cat. # C10619), Tyramide SuperBoost Kit with Alexa Fluor 488 or Alexa Fluor 647 conjugated to Tyramide (Cat. # B40936), and ProLong Gold anti-fade reagent with 4, 6-diamidino-2-phenylindole (DAPI) (Cat. # P36935) were purchased from Molecular Probes. Donkey normal serum (Cat. # Ab7475), goat normal serum (Cat. # ab156046), recombinant mouse FGF2 protein (Cat. # ab50235) and 5-Bromo-2'-deoxyuridine (BrdU, Cat. # ab142567) were purchased from Abcam. Streptavidin/Biotin Blocking Kit (Cat. # SP2002) was purchased from Vector Laboratories. Surveyor nuclease was purchased from Integrated DNA Technologies (Cat. # 706020, Coralville, IA). QIAquick Gel Extraction Kit and DNeasy DNA extraction kit were from QIAGEN. Isofluorane vaporizer was purchased from VetEquip Inc. (Livermore, CA, and USA). Bayer Contour Glucose Test Strip (Cat. # 56-7080) and glucose meter (Cat. # 567189) were bought from Save Rite Medical.

Table 1. Antibodies

Antibody	**Vendor, Catalog #**	**Host, clonality**	**Dilution**
Anti-α-MSH	Abcam, Cat. # ab123811	Rabbit, polyclonal	1/1000
Anti-NeuN	Abcam, Cat. # Ab128886	Rabbit, polyclonal	1/1000
Anti-rabbit (Cy5)	Jackson Immunoresearch, Cat. # 711-175-152	Donkey, polyclonal	1/500
Biotin-SP-Affinity Pure Anti-Rat	Jackson Immunoresearch, Cat. # 112-065-143	Goat, polyclonal	1/200
Anti-GFP	Abcam, Cat. # Ab13970	Chicken, polyclonal	1/1000
Anti-Chicken (Alexa Fluor® 488)	Abcam, Cat. # ab150169	Goat, polyclonal	1/1000

Anti-GRP78	Abcam, Cat. # ab21685	Rabbit, polyclonal	1/300
Anti-PSD95	Abcam, Cat. #: ab18258	Rabbit, polyclonal	1/1000
Anti-HA	Roche, Cat. # 11867431001	Rat, monoclonal clone 3F10	1/500
Anti-BrdU	Rockland, Cat # 600-401-C29	Rabbit, polyclonal	1/1000
Anti-doublecortin	Abcam, Cat # Ab153668	Chicken, polyclonal	1/500
Anti-Cox IV	Abcam, COXIV Cat #ab16056	Rabbit polyclonal	1/1000
Anti-KDEL	Enzo, Cat# ADI-SPA-827	Mouse, monoclonal	1/1000

Animals

MC4R-HA+/- mice. CRISPR/Cas9 gene-editing technology was used to insert two copies of the human influenza hemagglutinin peptide (2XHA) at the C-terminus of the endogenous MC4R. The sequence of the DNA encoding a 20 nucleotides guide RNA (gRNA) targeting the 3'end of murine MC4R DNA coding region on chromosome 18 was designed using the C57BL/6 mouse MC4R DNA sequence obtained from https://www.ncbi.nlm.nih.gov/nuccore/NC_000084.6?report=genbank&from=66857705&to=66860487&strand=true. The DNA oligonucleotide encoding the gRNA was synthesized with added BbsI restriction site at the 5' overhang and subcloned into the BbsI site of pX-330 vector, which contains the scaffold RNA and the Cas9 nuclease according to the published protocol (Cong et al., 2013). To insert the 2XHA sequence, a single-stranded ultramer (CT*G*AGGAAAACTTTCAAAGAGATCATCTGTTTCTATCCTCTGGGAGGCATCTGTGAGTTGTCTAGCAGGTATTACCCATACGATGTTCCAGATTACGCTTATCCATATGATGTTCCAGATTATGCTTAAGTGGGGGACAGAGTGCAAACTAGGTAGATACCTGCAGACTTTGTCACTCTGGCCCGATCTGAGCAGTG*T*AC, where *denotes the phosphorothioate) containing the DNA encoding 2XHA (head to tail) flanked by 72 nucleotides homologous to the 3' region of MC4R locus was designed and ordered from Integrated DNA Technology (IDT). The ultramer and pX-330 plasmid containing the DNA encoding the gRNA injected into C57BL/6 zygotes by the UAMS Genetic Models Core. To genotype the founder mice, genomic DNA was extracted from tail snips by using the DNeasy DNA extraction kit following the manufacturer's instructions. The region corresponding to the 3' of MC4R genomic DNA was amplified by PCR using 5'- CTTTCTCCATTTACTGTTCTACATCTCTTGCC-3' as the forward primer and 5'-GTGACAAAGTCTGCAGGTATCTACCTAG-3' as the reverse primer. The PCR products were run on a 2% agarose gel. The insertion of 2XHA was indicated by the presence of a higher molecular weight band corresponding to the insertion of 54 bp encoding 2XHA. The gel containing the upper molecular weight band was excised, and the DNA was purified from the gel by using the QIAquick Gel Extraction Kit following the manufacturer's instructions. The purified PCR product was sequenced at the UAMS DNA sequencing facility. One male founder mouse harboring the desired sequence was crossed with C57BL/6J female mice to obtain a colony of MC4R-HA+/- mice and then a colony of MC4R-HA+/+ mice. MC4R-HA+/- mice used for the experiments are derived from crossing of mice from the MC4R-HA+/+ colony to mice from the C57BL/6J mice (Cat. # 000664, The Jackson Laboratory), which are kept as colony at UAMS vivarium.

Sapphire mice: Mice that express GFP under the MC4R promoter (MC4R-GFP transgenic mice, Cat. # JAX 008323) were purchased from The Jackson Laboratory (Liu et al., 2003).

Sim1-Cre $^{+/-}$: Rosa-mEGFP$^{+/+}$ mice: the mice were generated as previously described by breeding Sim1-Cre$^{+/-}$ mice (Tg(Sim1-Cre) 1 Low L/J mice Cat. # 006451, The Jackson Laboratory) expressing Cre-recombinase under the Sim1 promoter REF with Rosa-mEGFP$^{+/+}$ mice (Gt(ROSA-MEGFP)26Sortm4(ACTB-tdTomato,-EGFP)Luo/J (Cat. # 007676, The Jackson Laboratory) (Muzumdar et al., 2007), to obtain a colony of Sim1-Cre $^{+/-}$: Rosa-mEGFP$^{+/+}$ mice.

Sim1-Cre $^{+/-}$: Rosa-mEGFP$^{+/+}$: MC4R$^{+/-}$ mice

Sim1-Cre $^{+/-}$: Rosa-mEGFP$^{+/+}$: MC4R$^{+/+}$ mice were obtained by first crossing MC4R-HA$^{+/+}$ mice with Rosa-mEGFP$^{+/-}$ to obtain Rosa-mEGFP$^{+/+}$: MC4R$^{+/+}$ and then by crossing these mice with with Sim1-Cre $^{+/-}$ mice.

Animal care and diet

All mice were bred, housed, and conditioned with low fat (LF) and HF diets in the University of Arkansas for Medical Sciences (UAMS) vivarium. Mice were housed in a temperature-controlled environment with 12h: 12h light-dark cycle, “lights on” at 0600 h, and "lights off" at 1800 h and given *ad libitum* access to food and water. Each shoebox cage housed 2-5 mice and had the addition of one “mouse hut” per cage for enrichment. UAMS veterinarians checked on the mice daily to monitor their health. Mice pups were genotyped at day 19-21 of age. The DNA used for genotyping was extracted from a small piece of tail (<2 mm). Mice were weaned at 21 days of age. No randomization or blinding methods were used to assign mice to different experimental groups. Eight-week-old mice were fed in parallel either with D12450H LF diet (3.82 kcal/g, fat = 10 kcal %) from Research Diets, Inc. or with the custom HF diet D15012001 (4.70 kcal/g, fat = 45 kcal %) from Research Diets, Inc. as described previously (Nyamugenda et al., 2019) and Table 2. Bodyweight and food intake were recorded every week. The UAMS Institutional Animal Care and Use Committee (IACUC) approved the protocol used for the animal studies (AUP FILE approval #: 3788).

BrdU injection

For experiments involving BrdU injections, each mouse received an intraperitoneal injection of BrdU solution (50 mg/kg body weight) by using a 500 µl BD insulin syringe equipped with the BD Micro-Fine IV Needle (U-100, 0.35 mm (28G) x 12.7 mm) (1/2)). Each mouse was injected once per day at 3 PM for seven days.

Food intake

Male and female mice on LF and HF diets were housed 2-5 mice per cage with *ad libitum* access to food and water. Three to four cages were used for each group. Food intake per cage was measured every week by subtracting the grams of the food remaining in the cage from the grams of food left in the cage the previous week. On average, 25 g of food per mouse was left in the cage every week to ensure that mice do not run out of food. The average weekly food intake per mouse was calculated by dividing the amount of food eaten per cage (in grams) by the number of mice in the cage. To calculate caloric intake per mouse, the amount of food in grams was multiplied by the amount of kcal/g of food

Table 2. Low fat diet (LFD) and high fat diet (HFD)diet.

Mouse diet	D12450H	D15012001
	10 % LF diet	45% HF diet
Caloric Information		
Protein:	20% kcal	20% kcal
Carbohydrate:	70% kcal	35% kcal
Fat:	10% kcal	45% kcal
Energy Density:	3.82 kcal/g	4.7 kcal/g

Diet ingredients		
Casein	200.00 g	200.00 g
L-Cystine,	3.00 g	3.00 g
Corn Starch	452.20 g	72.8 g
Sucrose	176.80 g	172.80 g
Maltodextrin	75.00 g	100 g
Cellulose	50.00 g	50.00 g
Soybean Oil, USP	25.00 g	25.00 g
Lard	20.00 g	20.00 g
Palm Oil	0.00 g	157.5 g
Fatty acid profile		
Saturated (g)	10.1 g	80.2 g
Monounsaturated (g)	12.8 g	79.1 g
Polyunsaturated (g)	20.2 g	41 g
Total fat	43.1 g	200.3 g

Blood glucose

One end of the Bayer contour glucose test strip was inserted into the glucose meter. A drop of blood was collected on the other end of the strip, and the reading of the glucose meter was recorded. The process was repeated for a total of three readings per mouse. The data are reported as the average of the three readings.

Collection of blood from the retro-orbital sinus to measure leptin and insulin

Mice were brought to the laboratory from the UAMS vivarium for fasting and euthanasia. Mice were deprived of food for three hours before being euthanized. Each mouse was deeply anesthetized in the induction chamber connected to the isofluorane vaporizer. The oxygen flow meter was set to 1.5 liters/min, and the isofluorane vaporizer dial was set at the maximal level of 5%. When the mouse was laying on its side and breathing rhythmically, it was removed from the chamber. Deep anesthesia was monitored by paw pinch, tail pinch, and eye blink tests. Approximately 0.2 ml of blood was collected from the retro-orbital sinus using a capillary inserted at the medial canthus of the eye under the nictitating membrane, and the animal was immediately returned to the induction chamber connected to the isofluorane vaporizer.

Mouse fixation

Each deeply anesthesized mouse was removed from the induction chamber and placed on a tray with its face in the nose cone of a circuit to maintain the isoflurane/oxygen administration. Deep anesthesia was again monitored by paw pinch, tail pinch, and eye blink tests. The heart was exposed following an established protocol (Gage et al., 2012), and the mouse was perfused through the heart's left ventricle with heparinized saline (0.9% NaCl containing two units of heparin/ ml at a rate of 3-4 ml/min) for 30 min, and then with 4% formaldehyde in PBS, pH 7.4 for another 30 minutes. The brain for each mouse was harvested and post-fixed in PBS containing 4% formaldehyde for 48 hours at room temperature. The brain was washed with PBS and stored in a 20 ml scintillation vial containing PBS, 30% sucrose, and 0.01% sodium azide. The brain was kept at 4^{o} C until sank at the bottom before slicing it into 30 µm coronal sections.

Brain Sections

When the brain was at the bottom of the vial containing 30% sucrose solution, it was sliced into 30 µm coronal sections using a cryostat (Microm HM 550, Thermo Scientific). First, the cerebellum and the prefrontal cortex were removed using a razor blade. The brain was then embedded in the clear Optimal Cutting Temperature Compound (OTC) on the cutting block and put in the cryostat chamber (-20^{o}C) until the OTC medium turns

solid white (about 15-20 minutes). A Standard High-Profile Disposable Blade was inserted in the cryostat's blade holder, and the cryostat was set to 30 µm "fine cutting." The frozen brain on the cutting block was inserted in the cryostat's sample holder for cutting. The brain sections were collected in serial order and stored in a 24 well plate containing PBS and 0.01% Sodium azide at 4°C.

Selection of the brain sections used in the study

Serial adjacent brain sections, including the PVN, the nucleus of the lateral olfactory tract (LOT), Supraoptic nucleus (SON), (Bregma -0.70 to -1.06 mm, and the arcuate nucleus (Bregma -1.22 to -1.94 mm) were used in the study. Sections of male mice treated with LF and HF diets were immunostained at the same time. The same protocol of staining was used for female mice. Male and female mice experiments were not carried out in parallel.

Immunostaining

For all the staining steps, sections were floating in a 24-well plate shaking on a plate shaker set at 200 rounds per minute (rpm) unless noted otherwise. Each well contained one section. From each step to the next, the section was transferred from one well to another using a small paintbrush. Each section was incubated with 1 ml of 0.5% Triton x-100 in PBS for 1h at room temperature (permeabilization step). Each section was then incubated for 1h at room temperature in 500 µl of PBS containing 0.1% Triton x-100 (PBST) and 10% of normal serum from the species where the secondary antibody was raised. Each sample was incubated for 48 hours at 4°C with 300 µl of the primary antibody diluted in PBST containing 1% BSA. Each section was washed four times for 10 minutes with 1 ml of PBS at room temperature and then incubated with 300 µl of the secondary antibody diluted in PBST and 1% BSA (PBST/BSA) overnight at 4°C. Each section was washed four times with PBS for 10 minutes each at room temperature and counterstained using 1 ml of 300 nM DAPI for 15 minutes at room temperature in the dark. Each tissue was washed three times for 5 minutes each and transferred to gelatin-coated microscope slides. Tissues on microscope slides were dried in the dark for 15 minutes before adding 20 µl of 1,4-diazabicyclo [2.2.2]octane (DABCO) mounting medium (40 ml containing 100 mg DABCO dissolved in 10 ml PBS with the addition of 30 ml glycerol). The coverslip was sealed using nail polish and left to dry in the dark.

Detection of MC4R-HA in brain sections

Each brain section was incubated with 1 ml of 0.5% Triton X-100 in PBS for 1 hour at room temperature on a 24-well plate on a plate shaker set at 200 rpm. Then sections were transferred to a well containing three drops of 2% hydrogen peroxide (using the dispensing bottle from the Tyramide SuperBoost™ Kit. The plate was tilted on one side to make sure that sections were covered entirely with the solution and incubated without shaking for 1 hour at room temperature. Each section was then washed three times with 1 ml PBS for 10 minutes at room temperature on the plate shaker set at 200 rpm. Nonspecific binding was blocked by incubating each section for 1 hour at room temperature in blocking buffer (500 µl of 10% normal goat serum in PBST) on the plate shaker set to 200 rpm. To block endogenous biotin each section was transferred to a well containing the "Streptavidin Solution" from the Streptavidin/Biotin Blocking Kit (3 drops using the drop bottle). Sections were incubated for 30 minutes at room temperature without shaking. Sections were washed 3 times with PBS. Sections were transferred to a well containing and the "Biotin Solution" from the Streptavidin/Biotin Blocking Kit (3 drops using the drop bottle) for 30 minutes at room temperature without shaking. Each section was washed three times with 1 ml of PBS for 10 minutes each on the plate shaker set at 200 rpm. Each section was then incubated with 300 µl of rat monoclonal anti-HA High-Affinity primary antibody diluted 1/500 in PBST/BSA) for 48 hours at 4° on the plate shaker set at 200 rpm. Each section was washed four times with 1 ml of PBS for 10 minutes each on the plate shaker on the plate shaker set at 200 rpm at room temperature. Each section was incubated overnight at 4° with 300 µl of Biotin-SP-Affinity Pure Goat Anti-Rat IgG secondary antibody diluted in PBST/BSA on the plate shaker set at 200 rpm. Each section was

washed four times for 10 minutes each with 1 ml of PBS at room temperature on the plate shaker set at 200 rpm. Sections were individually transferred to a well containing three drops of streptavidin conjugated to HRP from the Tyramide SuperBoost™ Kit. Sections were incubated for 1 hour at room temperature without shaking. Each section was washed four times with 1ml PBS for 10 minutes each at room temperature on the plate shaker set at 200 rpm. During the last wash, the following solutions were prepared following the Tyramide SuperBoost protocol: 1) 100 X H_2O_2 solution, by adding one drop of 3% H_2O_2 to 1 ml of distilled water; 2) 1 X Reaction buffer, by adding one drop of 20X Reaction buffer to 1 ml dH_2O. The 100 x Tyramide stock solution using Tyramide SuperBoost™ Kits with Alexa Fluor 488 (or with Alexa Fluor 647) was prepared in DMSO from Tyramide SuperBoost™ Kit following manufacturer instruction. Then, the tyramide working solution was prepared according to the following table.

Tyramide working solution Components	Number of wells (1 section per well)				
	2	4	6	8	10
100X Tyramide stock solution	2.5 µl	5 µl	7.5 µl	10 µl	12.5 µl
100X H_2O_2 solution	5 µl	10 µl	15 µl	20 µl	25 µl
1X Reaction buffer: from 2	500 µl	1000 µl	1500 µl	2000 µl	2500 µl

The Reaction stop reagent provided in the Tyramide SuperBoost™ Kit was prepared by diluting the stock solution 1:11 in PBS (100 µl of the reagent in 1ml of PBS). Each brain section was individually transferred to a well containing 250 µl tyramide working solution. Care was taken to make sure that the section lays flat and is covered with the solution. The section is incubated individually for 6 minutes without shaking. Then 250 µl of the diluted Reaction stop reagent was added to the well to stop the reaction. The procedure was repeated for every section. Sections were then washed four times with 1 ml PBS for 5 minutes, each while shaking on the plate shaker at 200 pm. Tissues were transferred to gelatin-coated microscope slides and dried in the dark before adding 20 µl DABCO to each section. The coverslip was mounted and sealed with nail polish.

BrdU staining of brain sections.

Each brain section was incubated with 1 ml of 0.5% TritonX-100 in 1X PBS for an hour at room temperature. Each section was then incubated in 1 ml of 2 N HCl at 37 °C for 30 min. The section was incubated with 1 ml of 0.1 M boric acid (pH 8.5) at room temperature for 20, followed by three washes with 1 ml PBS for 5 minutes each at room temperature. Each section was blocked in 500 µl of 10% donkey normal serum for an hour at room temperature followed by incubation with 300 µl of rabbit anti-BrdU primary antibody diluted 1:1000 in PBS containing 0.1 mg/ml ovalbumin, 0.1% TritonX-100, and 0.01% Na azide for 48 hours at 4^{o}C. The section was washed four times with 1 ml PBS for 10 minutes each and incubated with 300 µl of donkey anti-rabbit secondary antibody conjugated to Cy5 overnight at 4^{o}C and then washed four times with 1 ml PBS for 10 minutes each at room temperature. Each section was counterstained with 1 ml of 300 nM DAPI for 15 minutes and then washed three times with 1 ml of PBS at room temperature. Each section was transferred to a gelatin-coated microscope slide and dried in the dark before adding the mounting medium and coverslip. All incubations were carried out on a plate shaker set at 200 rpm. Sections were imaged using Olympus Fluoview FV1000 microscope.

Nile red staining of liver sections

Livers were harvested from the same animals immediately after the brain. After 48 hours post-fixation in PBS containing 4% formaldehyde, each liver was washed 3 times with PBS and stored in PBS containing 30% sucrose and 0.01% sodium azide in a 50 ml conical tube and kept at 4^{o} C for the following 48 hours, when the tissue sank to the bottom of the tube (some livers obtained from mice exposed to HF diet do not sink in 30%

sucrose solution). The livers were sectioned into 30 µm sections using the same protocol used for sectioning the brain. Each free-floating liver section was permeabilized using 1ml of 0.5% TritonX-100 in PBS for an hour at room temperature on a plate shaker set at 200 rpm. Each liver section was then incubated with 1 ml of 0.5 µM Nile Red for an hour at room temperature on a plate shaker set at 200 rpm followed by four washes with 1 ml of PBS for 10 minutes each. Each liver section was incubated with 1 ml of 300 nM DAPI for 15 minutes washed three times with 1 ml PBS for 5 minutes each. Each liver section was then transferred to a gelatin-coated microscope slide dried in the dark before adding the DABCO mounting medium and the coverslip. Sections were imaged using Olympus Fluoview FV1000 microscope.

Confocal microscopy

Images of the brain and liver sections were taken using a confocal microscope (Olympus Fluoview FV1000) equipped with 20 X/0.85 N.A Plan Apochromatic oil objective. Images were collected as a Z-stack of 8 optical slices of 3.0 µm thickness. Each Z-stack was converted into a two-dimensional maximum intensity projection image (MIP) by using the Olympus software. Higher magnification images were taken with the 60X/1.42 N.A Plan Apochromatic oil objective. All images of the same experiment were obtained with identical acquisition parameters.

Super-resolution microscopy

Images for analyzing the size of mitochondria and mitochondrial coverage area were taken using an inverted Zeiss ELYRA PS1 super-resolution microscope. Images were collected as a series of Z-stack of 12 optical slices using an alpha Plan-Apochromatic 100X/1.46 oil objective. The GFP in Sim1/MC4R neurons was detected by using a 488 nm laser, and COXIV was detected using a 642 nm laser. The 12 slice Z-stack was collected in Zeiss Zen Black software set to 3 grating rotations. Each optical slice was 2 µm resulting in z depth of 24 µm. For experiments that required imaging on different days, acquisition parameters were reloaded to ensure consistency. Images were processed using a proprietary structured illumination in Zen Black software. Structured illumination images were converted into 2D MIP images in XY projection and exported as TIFF files using Zeiss Zen Blue software.

Preparation of primary hypothalamic neurons and treatment with palmitate.

Primary cultures of hypothalamic neurons were prepared from 4 to 6-week old C57 and Sim1:Rosa mice fed ad libitum prior to sacrifice. Male and female mice (n = 6-8) were killed by CO_2 asphyxiation. All solutions, sterilized by filtration through 0.22 were equilibrated with 95% O2, 5% CO2. All glasswares, plasticwares and instruments are sterile. Brains were extracted and individually placed into 0.5 ml per well ice-cold Neurobasal Medium containing Neurobasal, pyruvate 0.23 mM, glucose 5 mM, and Penicillin, 100 IU, Streptomycin 100 µg/mL. For each brain, 1 brain section of 2 mm was cut using a Stoelting stainless steel brain matrix, with one single-edge blade placed anterior to the optic chiasm and the other blade placed anterior to the pons. From the coronal slice, a tissue rectangle of 2 mm width and 3 mm height centered around the entire 3rd ventricle to include the mediobasal hypothalamus and the PVN was dissected, the section was further cut by using single-edge blades into cubes of approximately 0.2 mm sides. The minced tissue was placed in an individual tissue culture well containing 0.5 ml EBSS with papain 20 U/ml, 1 mM EDTA, and 1mM DTT. The mixture was incubated in a tissue culture cabinet equilibrated with 95% air and 5% CO_2 for 15 min at 37 °C under agitation (OrbiShaker™ MP Orbital Microplate Shaker, 500 rpm), then DNAase was added from 1% w/v stock solution in EBSS to reach a final concentration of 0.005% w/v, and the mixture was further incubated in the tissue culture cabinet for other 15 min at 37 °C under continuous agitation. After digestion, the minced brain tissue in each well was triturated pipetting five times through a 1 ml pipet tip, pooled together, and filtered though a Corning Falcon™ Cell Strainer with 70 µm pores. The filtered cells were diluted to 6-8 ml by adding Neurobasal Medium and 6-8 aliquots of 1 ml were centrifuged in Eppendorf tubes placed on empty 10ml Falcon tunes to fit holders of an IEC clinical centrifuge and sample are spun for 2 min at 1000 RPM. Each pellet

was gently resuspended in 0.5 ml of Neurobasal Medium by pipetting five times through a 1ml pipet tip and transferred to another Eppendorf test tube containing 0.5 ml Neurobasal Medium with 10% FBS. Samples are centrifuged in a IEC clinical centrifuge for 2 min at 1000 RPM and each pellet was gently re-suspended in 0.3 ml of Hypothalamic Neuron Culture Medium containing Neurobasal Medium, 10% FBS, B27 diluted 1:50, 5 nM FGF2, and 0.5 µg/ml Vitamin D (from stock solution of 25 mg/ ml in DMSO) by pipetting five times through a 1ml pipet tip. The cell suspension in 0.3 ml volume is pipetted onto glass bottom culture dishes plates treated for 2h with 0.01% poly-lysine. The plates are transferred to the cell culture cabinet without agitation to allow for the cells to adhere to the glass bottom for 2h. Cells are washed by adding to the medium 1ml of HBSS, after gently swirling the medium for three times, the HBSS is replaced and the wash procedure is repeated once. Cells were cultured in 1 ml Hypothalamic Neuron Culture Medium for 10-14 days by replacing 0.5 ml of the medium with 0.5ml fresh medium every two days. On day 10-12 after plating, cells are incubated with and without 0.25 mM palmitate, prepared as described previously (Cragle and Baldini, 2014). To monitor mitochondrial membrane potential, MitoTracker™ Red is added to the medium to a final concentration of 200 nM and cells are further incubated for 30 min at 37 °C in the tissue culture cabinet. Live cells are washed twice with HBSS. Then cell medium is replaced with HBSS without phenol and containing pyruvate 0.23 mM and glucose 5 mM and cells are transferred to the stage of the Olympus microscope at room temperature to monitor fluorescence intensity of MitoTracker™ Red. Immediately after live cell microscopy, cells are fixed in formaldehyde and immunostained with antibodies against Cox. For some experiments, cultured neurons were derived from Sim1-Cre$^{+/-}$: Rosa-mEGFP$^{+/+}$ mice and immediately fixed to be immunostained with antibodies against PSD95.

Data analysis

Fluorescence intensity

Matching coronal brain sections from mice exposed to LF diet and HF diet were used for the analysis. MIP images were exported from the Olympus Fluoview FV10-ASW software (RRID: SCR_014215) as multi-tiff image files. The multi-tiff image files were opened with the ImageJ software (NIH, RRID: SCR_003070) as 16 bits RGB stack. The regions of interest (ROIs) with the same areas were drawn in matching sections of the PVN or arcuate nucleus of mice treated with LF or HF diet. The background for each image was subtracted by using the “subtract background” application under the “Image Processing” menu of the ImageJ. The raw integrated fluorescence intensity was measured within the ROIs. The results were exported from ImageJ as Excel files.

Number of NeuN, BrdU, and GFP-positive cells

Images were takes with the 20 X/0.85 N.A Plan Apochromatic oil objective. To count the number of NeuN and BrdU positive cells within the ROIs, multi-tiff images were opened with ImageJ software as 16 bits RGB stack. The ROI of the same area was drawn to outline the PVN. Using the “Analyze Particles” application within the Analyze menu of ImageJ, a table containing the number of particles (NeuN positive or BrdU positive cells) counts in the ROI was generated. The particle counts numbers were exported as Excel files and compared between the LF diet and HF diet. GFP positive cell counts were performed using the cell counter feature on ImageJ.

Number of cells expressing doublecortin and BrdU

Images were taken by using 60X/1.42 N.A Plan Apochromatic oil objective as a single XY scan. Four no-overlapping images were taken at each side of the 3rd ventricle, giving a total of 8 images per mouse (from two sides of the 3rd ventricle). Images were opened with the Olympus Fluoview FV10-ASW software and cells with doublecortin around BrdU positive nuclei were counted by using a manual cell counter. The data are reported as the sum of cell counts from 8 images per mouse.

Analysis of lipid abundance in the liver

To analyze lipid droplets in livers, MIP images were exported from Olympus Fluoview software, as indicated above. Multi-tiff images were opened in ImageJ as 16 bits RGB stack and adjusted by setting the lower threshold to 1000 pixels, and the upper threshold was automatically set to 3109 pixels. ROI was established to exclude holes at the central vein and destroyed areas of the tissues from the analysis. Using the "Analyze Particles" application within the analyze menu of ImageJ, the program generated a summary table containing the number of lipid droplets, and % area covered by lipid droplet. The table was exported as an Excel file to compare the average size of lipid droplets between mice exposed to LF diet and HF diet.

Abundance of mitochondria in Sim1/MC4R neurons

For measuring mitochondria abundance, confocal mages were exported from the Olympus Fluoview FV10-ASW software as a multi-tiff image format. The multi-tiff images were opened with ImageJ as 16 bits RGB stacks. ROIs were established around Sim1/MC4R neurons in the GFP channel, and the raw fluorescence integrated density within the ROI was measured in the COXIV (red) channel. The average raw integrated density of mitochondria per MC4R neuron, of at least 20 cells per mouse, was calculated and normalized.

Mitochondria size and mitochondria network

TIFF images were opened using ImageJ software and converted to 8 bits RGB stack. The ROIs were established by selecting areas around each cell in the GFP channel and adding the COXIV channel to the ROI manager application within the analyze menu. After selecting all cells, the lower threshold was set to 103, and the upper threshold was automatically set to 255 for all images. The area of each mitochondria particle was measured by using the "Analyze Particles" function to measure the area of the mitochondria in the COXIV channel. ImageJ generated a table containing the number of mitochondria particles and the area covered by each particle. The data were exported from ImageJ as an Excel file.

Statistical Analysis

The predefined criterion of the analysis has been to present all data, including outliers. All statistical analyses were performed using GraphPad Prism 6 software (GraphPad Prism, RRID: SCR_002798). Statistical significance was calculated by a two-tailed unpaired t-test with Welch correction on two groups or, where indicated, by two-way ANOVA with Holm-Sidak multiple comparison test on multiple groups. A value of $P < 0.05$ was considered statistically significant. Data were expressed as mean ± S.D unless noted otherwise.

Supplemental references

Cragle, F.K., and Baldini, G. (2014). Mild lipid stress induces profound loss of MC4R protein abundance and function. Molecular endocrinology (Baltimore, Md) *28*, 357y 367.
Gage, G.J., Kipke, D.R., and Shain, W. (2012). Whole animal perfusion fixation for rodents. J Vis Exp *65*, 3564.
Liu, H., Kishi, T., Roseberry, A.G., Cai, X., Lee, C.E., Montez, J.M., Friedman, J.M., and Elmquist, J.K. (2003). Transgenic mice expressing green fluorescent protein under the control of the melanocortiny 4 receptor promoter. J Neurosci *23*, 7143y 7154.
Muzumdar, M.D., Tasic, B., Miyamichi, K., Li, L., and Luo, L. (2007). A global doubley fluorescent Cre reporter mouse. Genesis *45*, 593y 605.
Nyamugenda, E., Trentzsch, M., Russell, S., Miles, T., Boysen, G., Phelan, K.D., and Baldini, G. (2019). Injury to hypothalamic Sim1 neurons is a common feature of obesity by exposure to highy fat diet in male and female mice. J Neurochem *149*, 73y 97.